AGU PUBLICATIONS

Geochemistry, Geophysics, Geosystems

RESEARCH ARTICLE
10.1002/2014GC005365

Special Section:
The Lithosphere-Asthenosphere System

Key Points:
- Joint modeling of Tibetan magnetotelluric and seismic data in petrologically consistent manner
- Lithosphere-asthenosphere boundary in central Tibet
- Estimates of water content in the Tibetan lithosphere

Correspondence to:
J. Vozar,
vozar@cp.dias.ie

Citation:
Vozar, J., A. G. Jones, J. Fullea, M. R. Agius, S. Lebedev, F. Le Pape, and W. Wei (2014), Integrated geophysical-petrological modeling of lithosphere-asthenosphere boundary in central Tibet using electromagnetic and seismic data, *Geochem. Geophys. Geosyst.*, *15*, 3965–3988, doi:10.1002/2014GC005365.

Received 1 APR 2014
Accepted 20 AUG 2014
Accepted article online 27 AUG 2014
Published online 24 OCT 2014

Integrated geophysical-petrological modeling of lithosphere-asthenosphere boundary in central Tibet using electromagnetic and seismic data

Jan Vozar[1], Alan G. Jones[1], Javier Fullea[1,2], Matthew R. Agius[1,3], Sergei Lebedev[1], Florian Le Pape[1], and Wenbo Wei[4]

[1]Dublin Institute for Advanced Studies, School of Cosmic Physics, Geophysics Section, Dublin, Ireland, [2]Institute of Geosciences, CSIC–UCM, Madrid, Spain, [3]Department of Physics, Faculty of Science, University of Malta, Msida, Malta, [4]School of Geophysics and Information Technology, China University of Geosciences, Beijing, China

Abstract We undertake a petrologically driven approach to jointly model magnetotelluric (MT) and seismic surface wave dispersion (SW) data from central Tibet, constrained by topographic height. The approach derives realistic temperature and pressure distributions within the upper mantle and characterizes mineral assemblages of given bulk chemical compositions as well as water content. This allows us to define a bulk geophysical model of the upper mantle based on laboratory and xenolith data for the most relevant mantle mineral assemblages and to derive corresponding predicted geophysical observables. One-dimensional deep resistivity models were derived for two groups of MT stations. One group, located in the Lhasa Terrane, shows the existence of an electrically conductive upper mantle layer and shallower conductive upper mantle layer for the other group, located in the Qiangtang Terrane. The subsequent one-dimensional integrated petrological-geophysical modeling suggests a lithosphere-asthenosphere boundary (LAB) at a depth of 80–120 km with a dry lithosphere for the Qiangtang Terrane. In contrast, for the Lhasa Terrane the LAB is located at about 180 km but the presence of a small amount of water in the lithospheric mantle ($<$0.02 wt%) is required to fit the longest period MT responses. Our results suggest two different lithospheric configurations beneath the southern and central Tibetan Plateau. The model for the Lhasa Terrane implies underthrusting of a moderately wet Indian plate. The model for the Qiangtang Terrane shows relatively thick and conductive crust and implies thin and dry Tibetan lithosphere.

1. Introduction

The Himalaya-Tibetan orogen is one component of the Alpine-Himalayan convergence zone created by the closure of the Tethys Ocean between Laurasia and Gondwana. This ongoing convergence is causing the rheologically more rigid Indian plate to collide with the weaker Tibetan Plateau, which comprises several terranes that were progressively accreted to Eurasia and is bounded to the north by the Kunlun Shan and to the south by the Himalayas [*Allègre et al*., 1984; *Dewey and Bird*, 1970; *Dewey et al*., 1988]. The tectonic history of Tibet is a prolonged history of terrane accretion lasting over 250 million years. Several deformation models of the region have been proposed in the literature to explain the elevation of the plateau; simple Argand-type models of an underthrusting Indian plate [*Argand*, 1924; *Ni and Barazangi*, 1984], lithospheric subduction [*Willett and Beaumont*, 1994; *Tapponnier et al*., 2001; *Tilmann et al*., 2003], rigid blocks models where the collision is dominated by strike-slip and normal faulting [*Molnar and Tapponnier*, 1977], and models where the convergence is accommodated by either crustal [*Royden et al*., 1997, *Shen et al*., 2001] or lithospheric [e.g., *Houseman and England*, 1986] ductile flows.

Crustal and upper mantle geophysical images of the Lhasa Block and Qiangtang Block in central Tibet (Figure 1), and of the Banggong-Nujiang Suture (BNS) separating the two, play an important role in developing our understanding of this continental collisional process [e.g., *Girardeau et al*., 1984; *Taylor*, 2003]. In particular, the presence and lateral and vertical extent of the Indian lithosphere beneath Tibet is highly debated in the literature [e.g., *Zhao et al*., 2011; *Searle et al*., 2011]. The InterNational DEep Profiling of Tibet and the Himalaya (INDEPTH) project in central Tibet revealed a large, high-velocity anomaly south of the BNS [*Tilmann et al*., 2003; *Li et al*., 2008a], consistent with Indian continental lithosphere underthrusting as far north

© 2014. American Geophysical Union. All Rights Reserved.

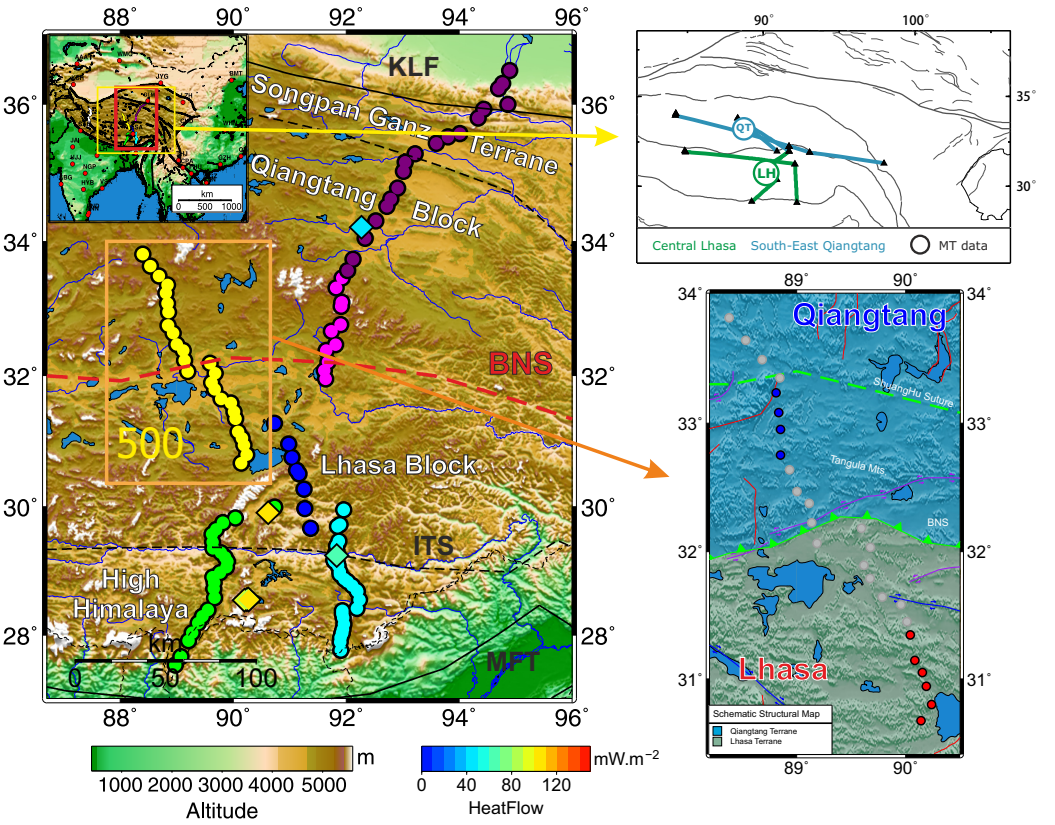

Figure 1. Maps showing the locations of INDEPTH MT profiles in Tibet. BNS—Banggong-Nujiang Suture, ITS—Indus–Tsangpo Suture; MBT—Main Frontal Thrust; KLF—Kunlun Fault; SS—Shuanghu Suture. The heat flow measurement sites are shown as diamonds with corresponding colors. (Top right) Map of seismic stations used for surface wave modeling in this manuscript. (Bottom right) Zoomed map of line 500 with highlighted sites from the Lhasa and Qiangtang Blocks used for analysis in this paper.

as the BNS in the location of the study area [*Owens and Zandt*, 1997; *Chen and Özalaybey*, 1998]. North of the BNS, the uppermost mantle has much lower seismic velocities, consistent with a thinner lithosphere [*Barazangi and Ni*, 1982; *Brandon and Romanowicz*, 1986; *Bourjot and Romanowicz*, 1992]. Although a high velocity anomaly is present beneath east-central Qiangtang at greater depths (below 150–200 km) it is likely to indicate subducted Indian rather than Tibetan lithosphere [*Agius and Lebedev*, 2013].

In this study, we use magnetotelluric (MT) data from the INDEPTH project line 500 [*Wei et al*., 2001; *Solon et al*., 2005] in central Tibet (Figure 1) together with surface-wave dispersion data, among other geophysical observables, to model the present-day thermal and compositional (i.e., major oxides and water) structure of southern and central Tibet. Our approach is based on a thermodynamically self-consistent framework using the software package LitMod [*Afonso et al*., 2008; *Fullea et al*., 2009; *Fullea et al*., 2011]. The program computes temperature and pressure distributions within the upper mantle and determines the stable mantle mineral assemblages given bulk chemical compositions. This approach allows us to: (i) define the bulk electrical resistivity, seismic velocity, and density model of the upper mantle based on laboratory studies for the most relevant mantle minerals, and (ii) compute synthetic geophysical observables that can be compared with observed data.

Integrated, self-consistent geophysical-petrological joint modeling of both seismological and electromagnetic data, simultaneously including the constraints offered by topography and heat flow, has the potential to yield superior inferences than using either of them independently due to their different sensitivities to temperature and composition (i.e., modal mineralogy and water content). Central Tibet, represented by the Lhasa and Qiangtang Blocks, offers an excellent natural laboratory for testing such approaches, given the high-quality seismological and MT data available as a consequence of the INDEPTH project and other studies [e.g., *Mechie et al*., 2004]. The resulting models derived from the

© 2014. American Geophysical Union. All Rights Reserved.

integrated approach are interpreted in terms of the tectonic evolution of the crust and upper mantle below the central Tibetan Plateau.

2. Geological Setting

The tectonic blocks that dominate the Tibetan Plateau were formed during Phanerozoic time as micro continental fragments accreted to the southern Asian margin. The Cenozoic Tibetan Plateau was created by the continent-continent collision between the northward moving Indian plate and Asia [*Dewey et al*., 1988], and the tectonics of the Plateau is dominated by four major terranes. From north to south these are the Songpan-Ganzi, Qiangtang, Lhasa, and Himalaya Terranes. All are separated by major sutures (Figure 1) [*Yin and Harrison*, 2000]. Terrane accretion was initiated in the late Permian when the northernmost subterrane of the Songpan-Ganzi Terrane accreted to the Kunlun (Tarim) Terrane of southern Asia along the Kun-Qinling Suture. Songpan-Ganzi terrane accretion was completed in the late-Triassic/Jurassic period. The Qiangtang Terrane is bounded to the north by the late-Triassic/Jurassic Jinsha Suture and to the south by the Banggong-Nujiang Suture (BNS) [*Girardeau et al*., 1984; *Taylor*, 2003]. The late-Jurassic BNS separates the Qiangtang and Lhasa terranes and trends approximately east-west across the interior of the Tibetan Plateau. Finally, the Himalaya Terrane sutured against the Lhasa Terrane along the (Yarlung-)Indus-Zangbo suture [*Yin and Harrison*, 2000]. The Indian plate to the south of the Himalaya Terrane continues to move northwards relative to Asia at about 5 cm per year [*Wang et al*., 2001; *Gan et al*., 2007].

The main Lhasa Block rock units exposed in the Lhasa Terrane are Jurassic–Cretaceous sedimentary and igneous rocks, volcano-sedimentary sequences, with minor Ordovician, Silurian, and Triassic limestones, the Cretaceous to early Tertiary Gangdese batholiths, and Triassic and Jurassic sedimentary deposits [*Kapp et al*., 2005; *Zhu et al*., 2009]. The Qiangtang Terrane is characterized by predominantly metamorphic rocks and Late Paleozoic (Carboniferous and Permian) shallow marine strata in the west, and by Triassic-Jurassic shallow marine carbonate rocks interbedded with terrestrial clastic and volcaniclastic strata in the east [*Yin and Harrison*, 2000].

There are several possible scenarios that would account for the accommodation of the intracontinental lithospheric convergence in this region. One of the basic convergence models is northward subduction of Indian, and possibly southward subduction of Asian, lithospheric mantle under Tibet [*Willett and Beaumont*, 1994; *Kind et al*., 2002]. *Tapponnier et al*. [2001] have proposed oblique subduction of Asian lithospheric mantle from the north that reactivated the Kunlun, Jinsha, and Banggong-Nujiang Suture (BNS) zones, with lateral extrusion in the form of the translation of discrete crustal blocks. Also, scenarios where the Indian Plate underthrusts the Himalayas and most of south and western Tibetan Plateau are widely proposed [*Argand*, 1924; *Ni and Barazangi*, 1984; *Owens and Zandt*, 1997]. In central Tibet as far north as the BNS, a subvertical high velocity zone down to a depth of 400 km is interpreted as downwelling Indian lithospheric mantle [*Tilmann et al*., 2003]. Homogeneous viscous lithospheric thickening [*Houseman and McKenzie*, 1981; *Dewey et al*., 1988], with convective removal of lithospheric mantle, has been proposed to explain the east-west extension of the Tibetan Plateau [*Molnar et al*., 1993, *Platt and England*, 1994], where the thickened lower lithosphere became convectively unstable and was replaced by upwelling hot asthenospheric material. Lithospheric thinning correlated with increasing topography in the Tibetan Plateau, as a consequence of rapid large-scale lithosphere removal, was also supported by joint 2-D modeling of gravity, topography, surface heat flow, and geoid data, using geological and seismic data in the crust as constraints [*Jiménez-Munt and Platt*, 2006; *Jiménez-Munt et al*., 2008].

However, from a petrological point of view the heterogeneous spatial and temporal distribution of the magmatism in the Tibetan Plateau is not indicative of a delamination process [*Searle et al*., 2011; *Williams et al*., 2004]. Tomographic models computed with surface waves in the data set [e.g., *Priestley et al*., 2008; *Schaeffer and Lebedev*, 2013] show low velocities in the upper few tens of kilometers of the mantle beneath central and northern Tibet, but high velocities in the upper mantle below. Some of the teleseismic body-wave tomographic models, however, do not show high velocities beneath central and northern Tibet [*Li et al*., 2008a], which motivated conceptual models with stacking of fragments of Indian lithosphere beneath the Himalaya and southern Tibet or lateral extrusion of Indian lithospheric fragments eastward [e.g., *Royden et al*., 2008]. Another scenario, proposed by *McKenzie and Priestley*, [2008], invokes thick lithosphere below

© 2014. American Geophysical Union. All Rights Reserved.

Tibet that may be forming a craton, with strong radiogenic heating within the thickened crust giving rise to the observed lower crustal shear-wave velocities.

3. Geophysical Setting

The lithosphere in the collision zone has been imaged across the whole Tibetan Plateau by several international geophysical projects, primarily seismological ones [PASSCAL: *Owens et al*., 1993; *Sol et al*., 2007; HI-CLIMB: *Hetényi et al*., 2007; *Nábělek et al*., 2009; INDEPTH: *Nelson et al*., 1996; *Zhao et al*., 2001; ASCENT: *Sandvol et al*., 2008; *Yang et al*., 2012]. The seismic discontinuity signatures of the Indian lower crust and lithosphere in receiver-function data extend north of the basal Main Frontal Thrust (MFT), with the Indian Moho disappearing close to the BNS for central Tibet at a longitude of around 85° [*Nábělek et al*., 2009]. There are interpretations based on seismic data of eclogitization of the Indian lower crust due to underthrusting [*Hetényi et al*., 2007], but these are not supported by gravimetric density modeling in central-south Tibet [*Bai et al*., 2013]. The receiver function studies of underthrusting Indian lithospheric mantle northern boundary represented by the deep north-south oriented profiles have been interpreted to suggest that the lithosphere does not follow the surface trace of major crustal suture zones [*Kind and Yuan*, 2010; *Zhao et al*., 2010]. North of the BNS, the central and northeastern parts of the Tibetan plateau exhibit high-frequency Sn-wave attenuation in the uppermost mantle [*Barazangi and Ni*, 1982; *McNamara et al*., 1995; *Barron and Priestley*, 2009], which suggests either thin Tibetan lithosphere, or a weak and warm lithosphere that could act as a deformable zone within the Indian-Asian collision. Surface-wave dispersion data require relatively low shear-wave speeds in the top few tens of kilometers of the upper mantle beneath central and northern Tibet, consistent with a warm and thin mantle lithosphere [*Tilmann et al*., 2003; *Liang et al*., 2012; *Agius and Lebedev*, 2013], which is in stark contrast with the cold, thick Indian lithosphere underthrusting beneath the Himalaya and southwestern Tibet [*Huang and Zhao*, 2006; *Li et al*., 2008a].

Crustal thickness in the Tibetan plateau is well constrained by several deep seismic soundings, refraction/reflection lines, and broadband teleseismics [*Ross et al*., 2004; *Zhao et al*., 2008; *Xiong et al*., 2009]. The deepest reported Mohorovičić discontinuity (Moho) is located in the West Kunlun (about 90 km) [*Wittlinger et al*., 2004] and the shallowest in the West Qinling (∼49 km) [*Gao et al*., 2005]. For our study regions, the Moho depths according to receiver-function studies [*Kind et al*., 2002; *Kumar et al*., 2006] and deep seismic soundings [*Zhao et al*., 2001; *Zhang and Klemperer*, 2010] are 66 km for the Qiangtang Terrane and 75 km for the Lhasa Terrane [*Kind et al*., 2002; *Li et al*., 2006].

A number of MT studies have been undertaken with the aim of describing the subsurface vertical and lateral distribution of electrical conductivity within the crust and uppermost mantle beneath Tibet. These were initiated with the Sino-French studies in the early 1980s [*Pham et al*., 1986] and were continued with INDEPTH since 1995 [e.g., *Chen et al*., 1996; *Wei et al*., 2001; *Solon et al*., 2005; *Spratt et al*., 2005; *Unsworth et al*., 2005; *Le Pape et al*., 2012; *Wei et al*., 2014]. Several zones of high electrical conductivity within the Tibetan crust south of the Kunlun Fault have been observed; the geometries and boundaries of some of these are associated with major tectonic sutures. The conductive zones are explained by various temperature-driven mechanisms, including aqueous (hydrothermal) fluids, partial melting, or a combination of the two [*Partzsch and Schilling*, 2000; *Li et al*., 2003; *Pommier and Le-Trong*, 2011]. Aqueous fluids and partial melt play an important role in active continental collision processes, for instance in the eclogitization of lower crust [*Leech*, 2001; *Zheng et al*., 2011] or channel flow in the middle and lower crust [*Bird*, 1991; *Royden et al*., 1997; *Clark and Royden*, 2000]. Two "channels" of higher conductivity observed in central and eastern Tibet were taken to indicate crustal flow and shearing as a result of deformation in the crust [*Nelson et al*., 1996; *Bai et al*., 2010] and upper mantle; widespread crustal low-velocity zones were detected [*Rapine*, 2003; *Klemperer*, 2006; *Xu et al*., 2007]. Conductance estimates from these zones, together with laboratory studies of partial melt conductivity, allowed estimation of effective viscosities with corresponding flow velocities [*Rippe and Unsworth*, 2010], and predicted flow velocities of the order 1 cm/yr.

4. Method

We undertake an integrated geophysical-petrological approach to forward model the topography, MT and surface-wave data by trial-and-error using the method of *Afonso et al*. [2008] and *Fullea et al*. [2009], encapsulated in their software code LitMod. This software combines petrological and geophysical modeling of

© 2014. American Geophysical Union. All Rights Reserved.

Table 1. Bulk Compositions Tested in This Study

	Mongolia: Average Garnet Peridotite[a]	Lhasa 1: Dry Fe-rich Harzburgite (ol/opx) (wt%)[b]	Lhasa 2: Dry Fe-rich Harzburgite (ol/opx/cpx) (wt%)[b]	Lhasa 3: Wet Fe-rich Harzburgite (ol/opx/cpx/sp/phl) (wt%)[b]	PUM M&S95 (wt%)[c]
SiO_2	44.59	43.44	43.2	42	45
TiO_2	0.14	–	–	–	0.201
Al_2O_3	3.48	0.44	0.96	2.24	4.45
Cr_2O_3	0.4	–	–	–	0.384
FeO	8.25	10.6	10.3	10.37	8.05
MnO	0.14	–	–	–	0.135
MgO	39.56	44.52	44.6	43.2	37.8
CaO	2.85	0.36	0.82	0.61	3.55
Na_2O	0.31	0.02	0.04	0.04	0.36
NiO	0.26	–	–	–	–
Total	99.98	99.28	99.92	99.5	99.93
Mg#	89.7	87.96	88.2	88.14	89.3

[a]Average garnet peridotite from Central Mongolia-Baikal from *Ionov* [2002 and references therein].
[b]Harzburgite averages in Sailipu (West Lhasa) from *Liu et al.* [2011].
[c]PUM stands for Primitive Upper Mantle, M&S95 refers to *McDonough and Sun* [1995].

the lithosphere and sublithospheric upper mantle within an internally consistent thermodynamic-geophysical framework, where all relevant properties are functions of temperature, pressure, and composition. The LitMod approach has been described in detail elsewhere [e.g., *Afonso et al*., 2008; *Fullea et al*., 2009, *Fullea et al*., 2011; *Fullea et al*., 2012; *Fullea et al*., 2014; *Jones et al*., 2014], to which the interested reader is referred; here we only present a general overview of the fundamentals for completeness. Below we discuss various pertinent aspects of the modeling. For more details on the MT and surface-wave calculations, the reader is referred to *Fullea et al*. [2011], *Jones et al*. [2012], and *Fullea et al*. [2012].

4.1. The Lithosphere-Asthenosphere Boundary

The lithosphere-asthenosphere boundary (LAB) has been characterized according to different geophysical proxy parameters: seismic velocities, seismic anisotropy, temperature, composition, and electrical resistivity [e.g. *Eaton et al*., 2009]. It divides the outermost, cold, relatively rigid lithospheric layer of the Earth from the warmer and rheologically weaker sublithospheric asthenospheric mantle. In this study, we assume a definition of the LAB that is based solely on the temperature and its gradient and compositional distributions. Accordingly, the lithospheric mantle is here defined (i) thermally, as the portion of the mantle characterized by a conductive geotherm, and (ii) compositionally, as the portion of the mantle characterized by different (more depleted) composition with respect to the fertile primary composition in the sublithospheric mantle (i.e., Primitive Upper Mantle (PUM) composition *McDonough and Sun*, 1995, see Table 1).

4.2. The Steady State Geotherm

The lithospheric geotherm is computed under the assumption of steady state heat transfer in the lithospheric mantle, considering a P-T-dependent thermal conductivity [*Afonso et al*., 2008; *Fullea et al*., 2009]. To avoid discontinuities in the thermal gradient at the base of the lithosphere, a buffer or transitional layer between the conductive lithosphere and the convective sublithospheric mantle is considered. This buffer zone, located immediately below the lithospheric domain, is assumed to be 40 km thick (or thicker if the lithospheric mantle is thicker than 60 km) and plays the role of a rheologically active layer where heat transfer is controlled by both conduction and convection, and is parameterized as a continuous linear superadiabatic gradient. In the sublithospheric mantle, the geotherm is given by an adiabatic temperature gradient required to lie within the range 0.35–0.6 C/km [see Appendix A2 in *Fullea et al*., 2009, for details].

4.3. Thermodynamic Framework

Stable mineral assemblages in the mantle are calculated using a Gibbs free energy minimization as described by *Connolly* [2005]. The composition is defined within the NCFMAS (Na_2O-CaO-FeO-MgO-Al_2O_3-SiO_2) major oxide system. All the stable assemblages in this study were computed using a modified version of the thermodynamic database of *Holland and Powell* [1998] [see *Afonso and Zlotnik*, 2011]. The density and seismic velocities in the mantle were determined according to the elastic moduli and density of each end-member mineral, as described by *Connolly and Kerrick* [2002] and *Afonso et al*. [2008]. Anelasticity effects are of primary importance to accurately determine seismic velocities, particularly at high

© 2014. American Geophysical Union. All Rights Reserved.

temperatures [e.g., *Karato*, 1993; *Cammarano et al*., 2003; *Afonso et al*., 2010]. Anelasticity is computed as a pressure-temperature-dependent correction to the anharmonic output velocities [e.g., *Minster and Anderson*, 1981; *Karato*, 1993; *Afonso et al*., 2005]. The effects of other parameters on the anelasticity correction applied here have been explored elsewhere [*Fullea et al*., 2012], with the conclusion that grain size and activation volume in the lower bounds of ranges based on laboratory observations [e.g., *Faul and Jackson*, 2005] predict too low-shear wave quality factor Qs with too low Vs velocities. The upper bounds indicate a moderate negligible increase in Vs compared to standard values of grain size and activation volume used in this study. The bulk electrical conductivity is computed according to modal mineral distribution, temperature, and water content [*Fullea et al*., 2011, *Jones et al*., 2012], based on conductivity models from laboratory experiments to measure the electrical properties of many of the mantle minerals under various conditions.

5. Geophysical Observables and Primary Crustal Modeling

The focus of this paper is on the first-order thermal and compositional structure of the lithospheric mantle beneath the two study regions in central Tibet, i.e., thicknesses and hydrous states of the lithosphere north and south of the BNS (Figure 1). However, crustal structures play a crucial role in MT and surface-wave data modeling, even for the long periods that are primarily sensitive to deep structure. Therefore, prior to the coupled geophysical-petrological modeling of the mantle, we independently inverted the MT and surface-wave data for the resistivity and seismic velocity distributions respectively in the thickened Tibetan crust. MT responses are insensitive to crustal density, and surface waves are less sensitive to density than they are to seismic velocities at depth. However, topography is extremely sensitive to assumptions made about crustal density and its distribution [see, e.g., *Jones et al*., 2014].

5.1. Magnetotelluric (MT) Data

MT data collected during Phase III of the INDEPTH project along line 500 (see Figure 1) are reexamined and remodeled in this study. In order to reduce unwanted local distortion effects in the original MT impedance tensors, dimensionality [e.g., *Simpson and Bahr*, 2005; *Martí et al*., 2009; *Jones*, 2012], and regional strike [*Groom and Bailey*, 1989] analyses of the data are required after primary processing. Based on the distribution of sites along the profile, we used the *McNeice and Jones* [2001] multisite, multifrequency extension of the Groom-Bailey MT tensor decomposition technique [*Groom and Bailey*, 1989] to determine the dominant geoelectric regional strike for several frequencies and Niblett-Bostick [*Jones*, 1983] depth ranges. The resulting magnetotelluric transverse electric (TE) and transverse magnetic (TM) mode data were decomposed to a newly defined regional azimuth angle of E10°S (i.e., N100°E) for line 500. The uncertainties for the TE and TM apparent resistivities and phases were determined by a bootstrap procedure involving hundreds of realizations of recovered parameters fitting decomposition models of measured impedance elements to determine the scatter of the values [*McNeice and Jones*, 2001]. The apparent resistivity and phase error floors are set to 3%. Corrections for static shift were applied based on previous 2-D MT modeling (Vozar et al., Three-dimensional structures and geometries of central Tibetan Plateau from INDEPTH magnetotelluric data, submitted to *Journal of Geophysical Research*, 2014). As a final analysis step, quality checks of the TM and TE decomposed data were performed by testing the consistency of the apparent resistivities and phases with theoretical predictions from the best fitting Rho^{+} model [*Parker and Booker*, 1996], as demonstrated by e.g. *Spratt et al*. [2005].

A subsection of the MT stations along the INDEPTH 500 line was selected for integrated modeling of the mantle structure (marked by circles in the north (purple – ii) and south (red - i) in Figure 1). Based on skin depth and consistency considerations, MT data for the TE mode, which is more sensitive to LAB depth than the TM mode [*Berdichevsky and Dmitriev*, 2008], in the Lhasa Block and the Qiangtang Terrane were selected for integrated modeling. The TE mode responses are induced by approximately east-west flowing currents that are aligned with the geological strike seen at the surface. Data from stations within the two groups (i.e., Lhasa and Qiangtang) exhibit significant similarities in their sounding curves (Figure 2). The layered one-dimensional (1-D) models (Figure 3) are imaging laterally continuous deep geoelectrical structures beneath the two regions. The 2-D model (Vozar et al., submitted manuscript, 2014) is presented in the last row of Figure 3 to show consistency with 1-D models. Earthquake data from the International Seismological Centre were taken between longitudes E88° and E90° and projected onto the profile plane. The earthquake hypocenter positions are plotted as open circles within the profile, where the diameter of circles indicates their magnitude [*International Seismological Centre*, 2012].

© 2014. American Geophysical Union. All Rights Reserved.

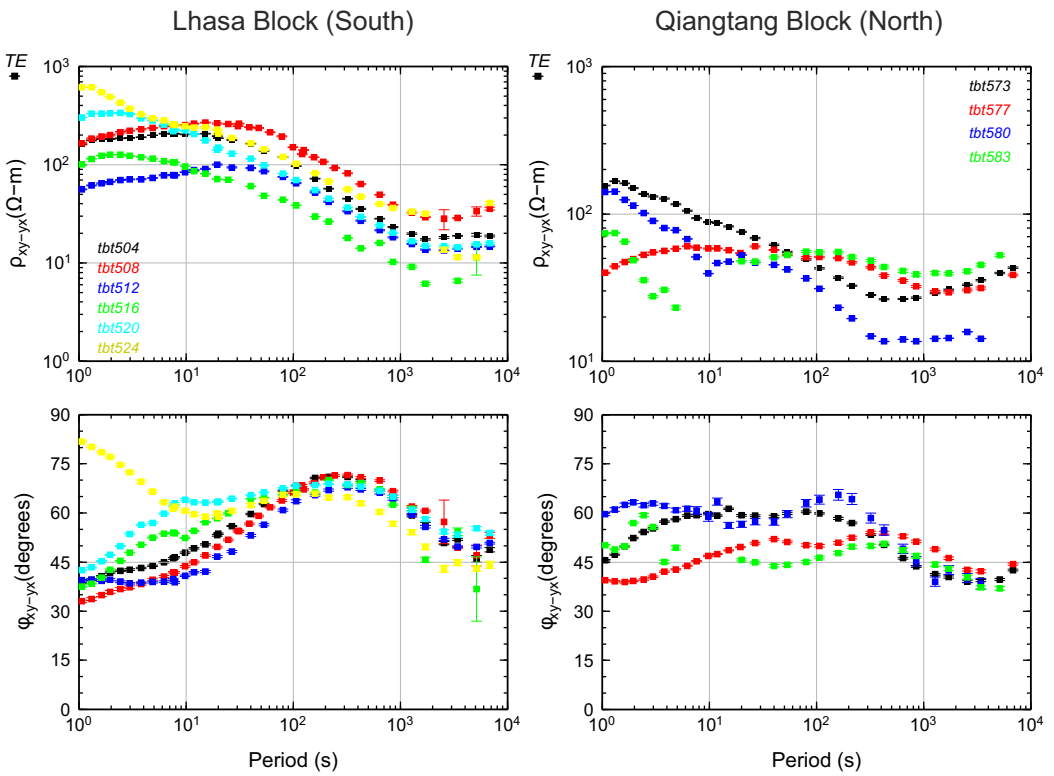

Figure 2. Apparent resistivities and impedance phases of the TE magnetotelluric mode decomposed to regional strike direction for selected sites in the Lhasa and Qiangtang Blocks. The data are used in integrated modeling.

We inverted INDEPTH MT data at the selected stations (Figure 2) using an Occam inversion scheme [*Constable et al.*, 1987] that solves the regularized problem by trading off data misfit and model roughness using Tikhonov regularization. Specifically, we used the Occam 1-D inversion of TE and TM modes of decomposed MT data as implemented in the WinGLink© package. For all stations, we used an identical starting model; a 100 Ωm layered halfspace. As described by *Berdichevsky and Dmitriev*, [2008] the pseudo-2-D model, created through stacking the individual 1-D models, shows that the 1-D TE models are more consistent from site to site along the profile than the TM models. The 1-D TE models at almost all sites are consistent as conductive structures in the crust and upper mantle can be followed laterally with varying thickness and depth (Figure 3). It is likely that 1-D TM inversion models are affected by distortion in the southern (Lhasa Block) and middle (BNS) parts of the profile due to the presence of the resistive Gangdese batholith.

In Figures 2 and 3, the 1-D models and primary MT data show the consistencies between the data and 1-D TE models. The impedance phases and apparent resistivities are very similar in the Lhasa Block at long periods (>30 s) that are sampling mantle structure. The selected 1-D models from the Qiangtang Block exhibit higher heterogeneity than those in the Lhasa Block, although again for the longest periods sampling the mantle (> 300 s) the sounding curves become very similar. We focused on the most robust stations, i.e. as far away as possible from the complicated structures in the BNS zone, with the deepest possible penetration. Other sites in Qiangtang were selected based upon their positions in the area between the Shuanghu Suture (dividing Qiangtang to eastern and western) and the BNS. This area better corresponds to the Qiangtang seismic data. 1-D models based on the averages of four 1-D models for the Lhasa Block and three models for the Qiangtang Block are shown in Figure 4. The error bars on the models in Figure 4 represent the standard deviation between the averaged models. The conductive layers visible in the mantle, denoted by the red arrows in Figure 4, are likely to be associated with the electrical LAB (eLAB). They are located at a depth greater than 200 km for the Lhasa Terrane, whereas for the Qiangtang Terrane they are located less than 180 km deep. For final integrated modeling, we selected the best quality MT data (TE mode) from selected sites, i.e. station 512 for the Lhasa Block and station 577 for the Qiangtang Block. The range of all models is presented as the gray background trace in the resistivity petrological models in Figures 5 and 6.

© 2014. American Geophysical Union. All Rights Reserved.

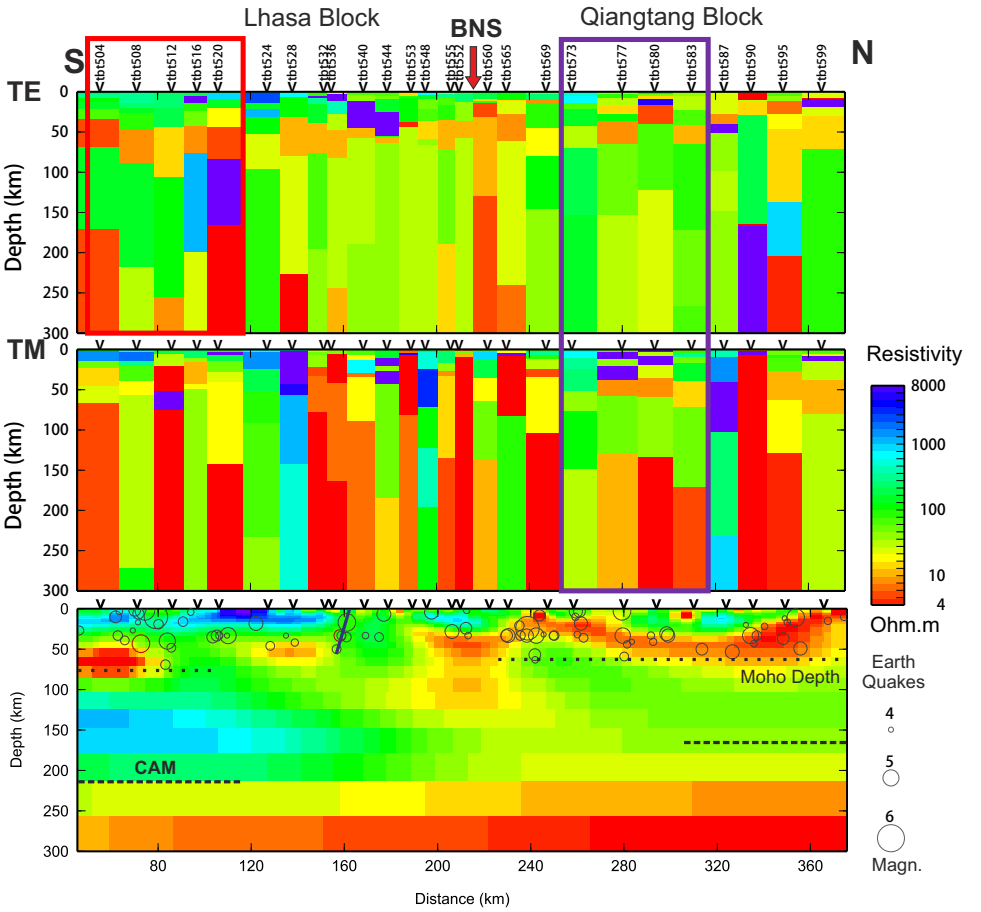

Figure 3. Pseudosections of 1-D models for all sites from line 500 for decomposed and static-shifted TE mode, TM mode, and Invariant data. Selected regions for final modeling are marked by red (the Lhasa Block or South) and purple (the Qiangtang Block or North) squares. In the last row, we present a 2-D model with earthquakes projected onto the profile (Vozar et al., submitted manuscript, 2014).

5.2. Surface-Wave (SW) Data

Both Rayleigh and Love waves, the two surface-wave types, are dispersive and sample deeper structure at longer periods. For example, Rayleigh waves sample the upper and middle Tibetan crust at 10–20 s periods and mainly the 70–150 km depth interval at 70–80 s periods, whereas Love waves are sensitive from the surface down to 40 km depth at the shorter periods (10–20 s) and from the surface to 100 km depth for the longer periods (70–80 s) [e.g., *Agius and Lebedev*, 2013]. Surface-wave measurements in broad period ranges can thus be used in order to resolve the trade offs between crustal and mantle structure in an inversion, in an analogous fashion to MT responses in different periods bands. Phase velocities of surface waves depend primarily on the composition and temperature of the crust and mantle, but also depend on anisotropic fabric within them. Measurements of both Rayleigh and Love wave velocities are required in order to determine radial anisotropy and derive the isotropic-average shear-wave speeds that are related directly to the temperature and composition of the rocks at depth.

Phase velocities of Rayleigh and Love waves in broad period ranges were determined recently for a selection of station-station pairs across Tibet [*Agius and Lebedev*, 2013] using a combination of cross-correlation and multimode-waveform inversion approaches, with data from stations of various recent broad-band experiments. The accurate, broadband interstation phase-velocity curves were computed by averaging over tens to hundreds of single-event measurements for each station pair, using earthquakes in different source regions. Dispersion curves from neighboring pairs of stations showed close similarity within a number of subregions within Tibet, including the central Lhasa and central Qiangtang terranes. The phase-velocity curves that we use here for these regions are averages over the phase-velocity measurements from the multiple station pairs within them (Figure 1).

© 2014. American Geophysical Union. All Rights Reserved.

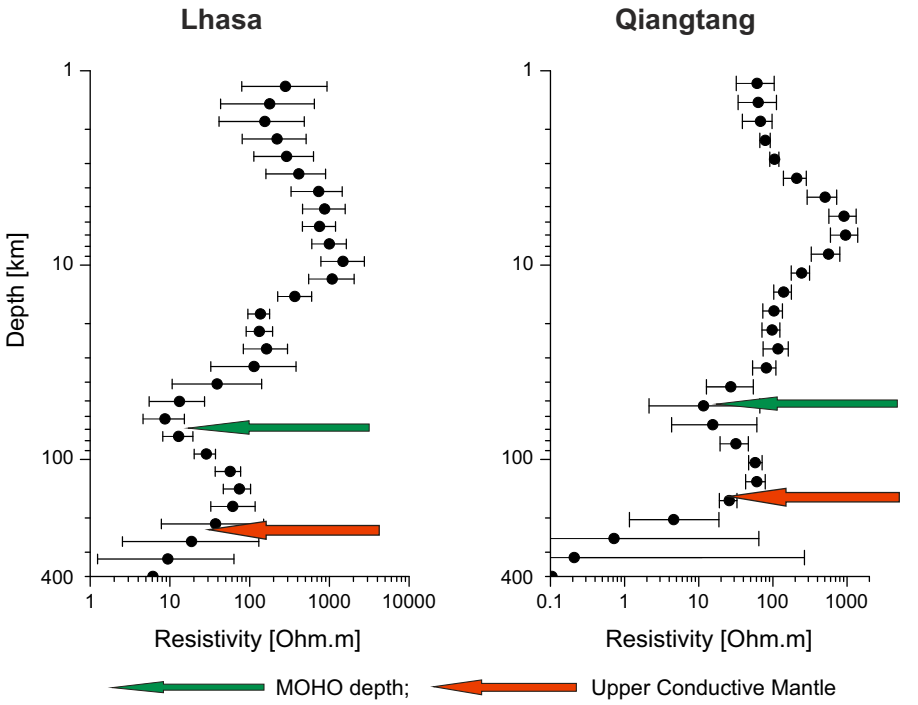

Figure 4. Averaged 1-D normal models created from the TE mode of sites 504, 508, 512, and 520 for the Lhasa Block and from the TE and TM modes of sites 573, 577, 580 for the Qiangtang Block. Error bars represent the standard deviation between the averaged models. The red arrows show a resistivity value 30 Ohm.m.

The Rayleigh-wave and Love-wave dispersion curves were inverted simultaneously for 1-D profiles of the isotropic-average shear speed Vs = (Vsh + Vsv)/2 and radial anisotropy, (Vsh − Vsv)/2, where Vsv and Vsh are the vertically and horizontally polarized shear speeds, respectively [*Agius and Lebedev*, 2013, and references therein]. Compressional velocity, Vp, which has a nonnegligible influence on the Rayleigh-wave phase velocity, was assumed isotropic. The models comprised seismic-velocity perturbations from the surface down to the shallow lower mantle, with the surface topography taken into account.

The inversion results are fundamentally nonunique, and a suite of models can fit the surface-wave data equally well [*Agius and Lebedev*, 2013]. In order to represent the crustal shear velocity and the radial anisotropy profiles beneath central Lhasa and central Qiangtang in the integrated modeling, we chose representative single models based on the low misfit they provided and on their smoothness (nonoscillatory depth dependence) (Figures 5 and 6, gray background lines).

5.3. Topography, Surface Heat Flow (SHF), Density, and Thermal Parameters

In addition to fitting the MT data and surface wave dispersion curves, we constrain our ranges of acceptable models to those that yield surface topography and surface heat flow values consistent with observations. The modeled topography has been taken from elevation information at MT sites (Lhasa: from 4750 to 5030 m, Qiangtang: from 4883 to 5023 m) and varies approximately ±200 m in the area around the modeled sites. The topography provides information on the integrated density of the lithosphere, including the crust. Our calculated values of surface heat flow (SHF) are compared with measurements in the Tibetan plateau and from the global data set [*Francheteau et al.*, 1984; *Jaupart et al.*, 1985; *Pollack et al.*, 1993; *Tao and Shen*, 2008]. Unfortunately, the coverage and quality of SHF data for central Tibet is poor (just one site in the Qiangtang Terrane) and they include measurements on lake bottoms. The high SHF in some parts of Tibet ($>$100 mWm^{-2}) has been attributed to shallow magma intrusions from metamorphic dewatering of the thickened Tibetan crust caused by radiogenic heating, and they yield little information on the mantle heat flow [*Jaupart et al.*, 2007]. Indirect thermal data provide seismic detection of the α-β quartz transition zone [*Mechie et al.*, 2004], which implies approximately 700°C at a depth of about 18 km north of the BNS (i.e. the southern Qiangtang block) and 800°C at a depth 32 km south of the BNS (the northern Lhasa block).

© 2014. American Geophysical Union. All Rights Reserved.

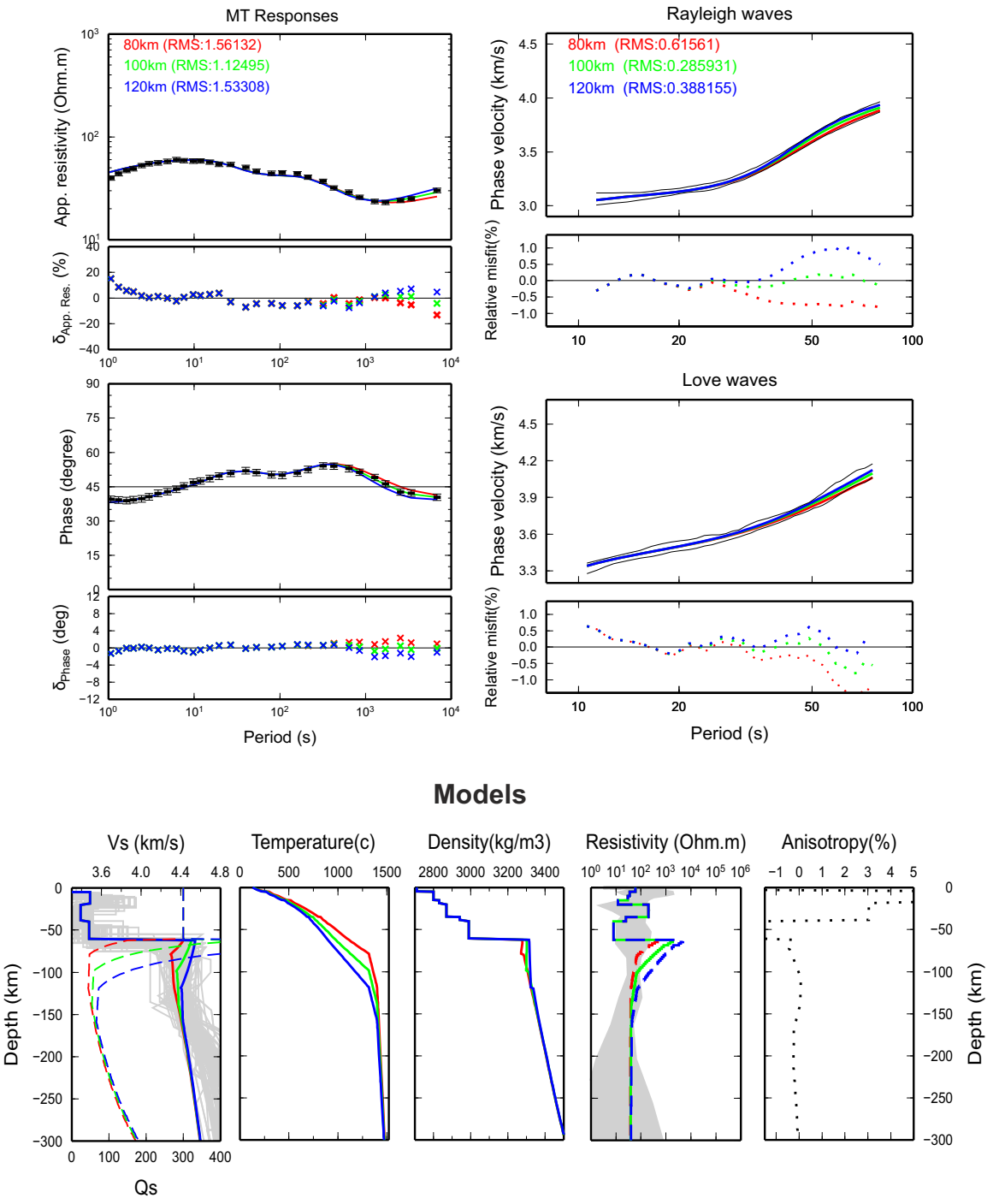

Figure 5. Integrated modeling of the Qiangtang region with dry standard mantle composition. (top) Fits of MT and seismic data for three (red—80 km, green—100 km, and blue—120 km) different LAB depths. (bottom) Corresponding calculated models of Vs velocities (dashed lines represent shear-wave quality factors Qs, gray lines represent all possible models based only on seismic modeling), temperature, density, resistivity (gray area—the range of all resistivity models based only on MT data), and anisotropy.

In order to constrain the density distribution within the lithosphere, inversions of surface-wave data need to incorporate additional information, such as surface topography (assuming local isostasy) [*Fullea et al.*, 2012]. The density distributions in our models are based on previous geophysical studies [*Jiménez-Munt and Platt*, 2006; *Jiménez-Munt et al.*, 2008; *Bai et al.*, 2013] and seismic velocities obtained along seismic profiles [*Zhao et al.*, 2001; *Haines et al.*, 2003; *Zhao et al.*, 2001; *Zhang and Klemperer*, 2010] in the study area by using the velocity-density relation of *Christensen and Mooney* [1995]. The average crustal density is an important

© 2014. American Geophysical Union. All Rights Reserved.

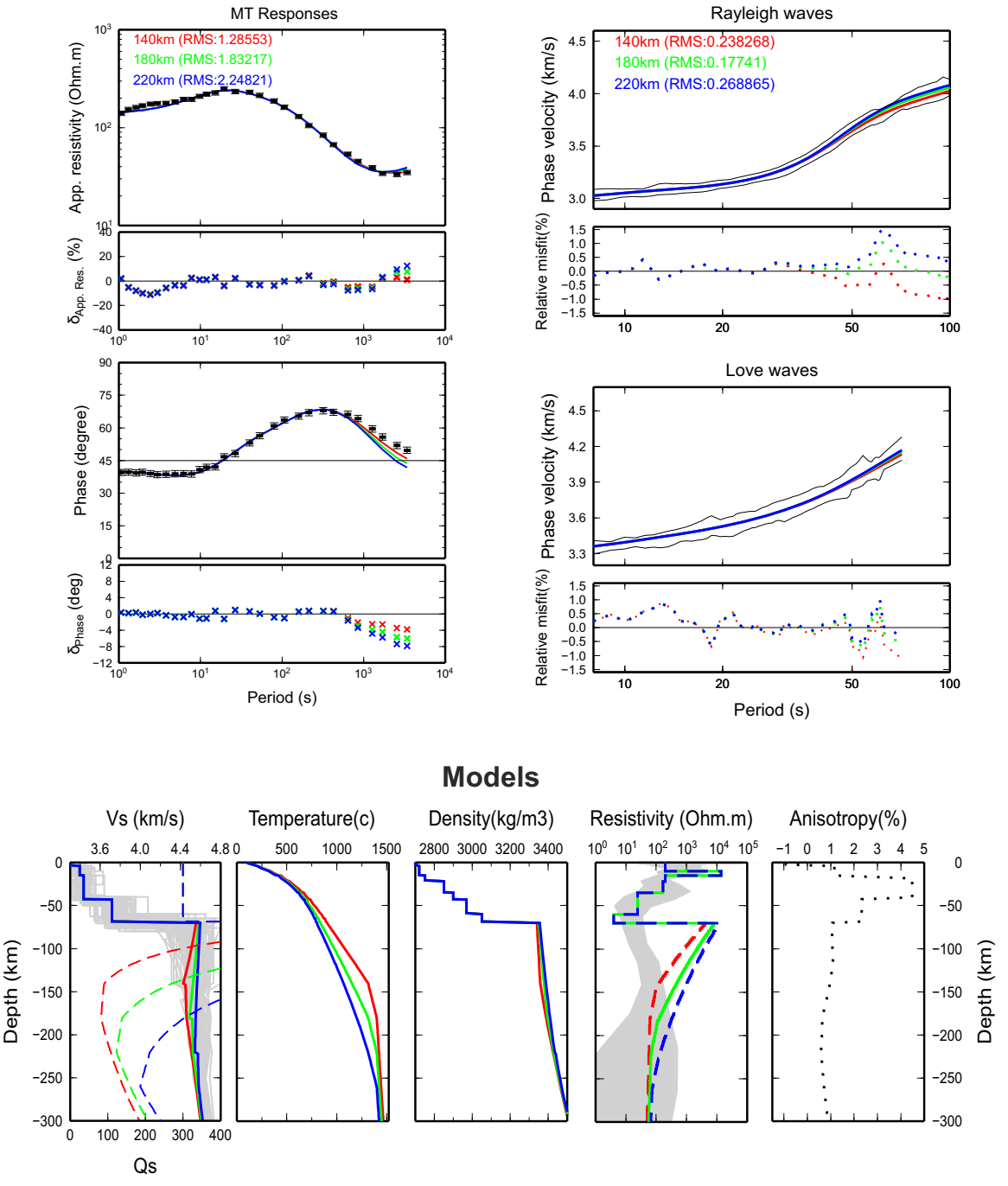

Figure 6. Integrated modeling of the Lhasa region with dry lithosphere composition. (top) Fits of MT and seismic data for three (red – 140 km, green – 180 km, blue – 220 km) different LAB depths. (bottom) Corresponding calculated models of Vs velocities (dashed lines represent shear wave quality factors Qs, gray lines represent all possible models based only on seismic modeling), temperature, density, resistivity (gray area—the range of all resistivity models based only on MT data), and anisotropy.

parameter for fitting modeled data and tests of density ranges are discussed below. The crustal thickness is based on previous seismic studies (see section 3), local isostasy balance considerations, and fitting of MT and surface-wave data, which is part of the mantle modeling (Figures 7a and 7b). In Table 2, we present the average main mechanical and thermal parameters (crustal density, radiogenic heat production coefficient, and thermal conductivity) for the Qiangtang and Lhasa Terranes used in our modeling. Other observables suitable for 1-D modelling (such as geoid heights) are affected in our case by strong 2-D and 3-D trends and are therefore not included here.

© 2014. American Geophysical Union. All Rights Reserved.

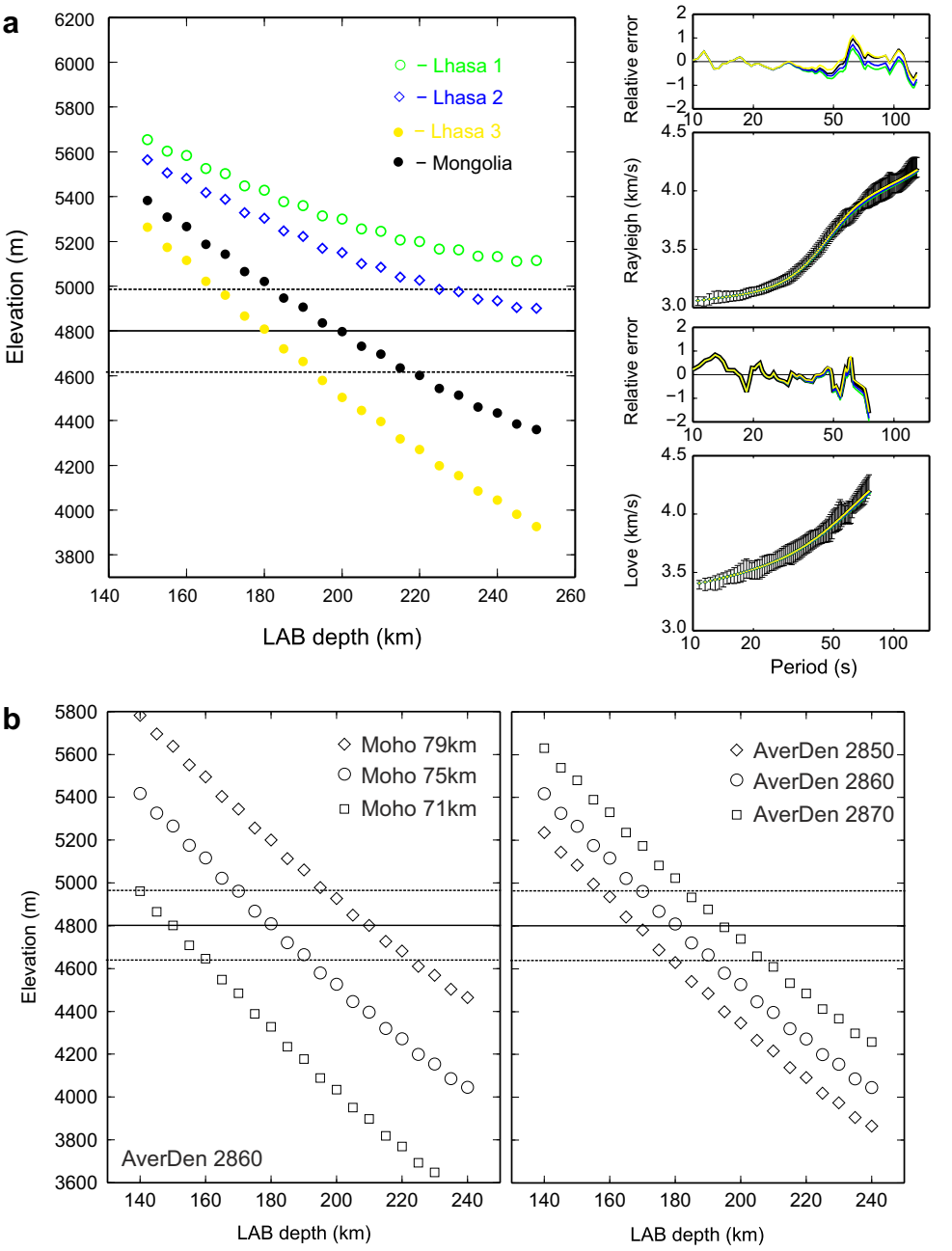

Figure 7. (a) Effect of various mantle compositions tested in the Lhasa Block (see Table 1). (left) Predicted topography versus LAB depth. (right) Predicted dispersion curves for Rayleigh (top) and Love waves (bottom) for a fixed LAB depth of 180 km. (b) Effect on the predicted topography in the Lhasa Block of varying the average crustal density (left) and Moho depth (right) for a fixed Lhasa 3 mantle composition (Table 1).

6. Lithospheric Mantle Modeling Results

In order to isolate the mantle contribution to the geophysical observables, we have assumed a fixed crustal structure (i.e., fixed crustal seismic velocities, electrical resistivity, and density) as described above (sections 6.1 and 6.2). Bulk mantle composition is a second-order parameter in MT and surface-wave computations with respect to temperature or water content [e.g. *Fullea et al.*, 2011; *Fullea et al.*, 2012; *Jones et al.*, 2012]. In this work, we consider different compositions based on xenolith data from western Lhasa [*Liu et al.*, 2011] as well as global average garnet peridotite values based on Asian mantle xenolith data [*Ionov*, 2002; *Barry et al.*, 2003] (Table 1). We selected xenoliths from Mongolia because they correspond to an average garnet

© 2014. American Geophysical Union. All Rights Reserved.

Table 2. Averaged Main Mechanical and Thermal Crustal Parameters Used for Modeling in This Study [*Jimenez-Munt et al.*, 2008; *Bai et al.*, 2013][a]

	Qiangtang			Lhasa		
	Densities (kg/m^3)	Radiogenic Heat Production (μW/m^3)	Thermal Conduction (W/(mK))	Densities (kg/m^3)	RGHP (μW/m^3)	Thermal Conduction (W/(mK))
Sediments	2600	2.5	2.5	2500	2.0	2.5
Upper crust	2750	2.0	2.5	2750	1.7	2.5
Middle crust	2940	1.0	2.3	2930	0.7	2.1
Lower crust	3000	0.2	2.1	3050	0.2	2.1

[a]The crust is composed of 10 layers with gradually increasing densities.

peridotite (typical Phanerozoic composition) only moderately depleted with respect to PUM composition of the sublithospheric mantle, whereas the xenoliths from Sailipu in west Lhasa are Fe-rich spinel harzburgites with varying amounts of water.

The presence of even small amounts (tens of ppm) of water in the mantle (i.e., hydrogen that upon bonding with oxygen atoms in the silicate structure forms measurable hydroxyl groups) plays an important role in its rheological and electrical properties [*Yuen et al.*, 2007; *Karato*, 2010; Fullea et al., 2011; *Jones et al.*, 2012]. The effect of water on the electrical conductivity of the upper mantle nominally anhydrous minerals is the cause of intense debate in the literature [e.g. *Dai and Karato*, 2009; *Yoshino*, 2010; *Karato and Wang*, 2013], but all laboratories are in agreement that water has a significant effect in enhancing conductivity by several orders of magnitude. Different laboratories have estimated the magnitude of the effect of the so-called proton conduction term in olivine (i.e., water related) on the electrical conductivity of olivine with rather different results [*Wang et al.*, 2006; *Yoshino et al.*, 2009; *Poe et al.*, 2010]. *Jones et al.* [2012] proposed a new model based on the above-mentioned lab studies plus additional geophysical and petrological constraints. However, recently *Jones* [2014] pointed out that none of the equations used by those authors to describe proton conduction is consistent with the Meyer-Neldel Rule (MNR), by which the preexponent term and the activation energy term are linearly related. Here, in order to be both inclusive and exhaustive and given that it is currently not known which water conduction model is correct, if any, we will consider three proton conduction models to estimate the amount of water in the Tibetan/Indian mantle, namely (1) *Wang et al.* [2006]; (2) *Yoshino et al.* [2009]; and (3) *Jones et al.* [2012].

We note that although water would have an impact on the mineral assemblage (i.e., hydrous phases) and seismic data (i.e., via seismic attenuation), at the scale of this study (ppm) its effects can be considered negligible on the seismic response. Therefore, the free parameters used in this study to characterize the lithospheric mantle are the LAB and Moho depth (controlling the geotherm) and the amount of water in the mantle (affecting the electrical resistivity distribution).

6.1. Qiangtang Terrane

For the northern part of line 500 (Figure 1), located in the Qiangtang Terrane, the best-fitting lithospheric model found, determined through forward trial-and-error fitting, is characterized by a relatively fertile and dry composition (Mongolian composition in Table 1) and a lithospheric thickness of around 100 km (Figure 5). The root-mean square (RMS) misfits between the observed and modelled geophysical data, representing reduced chi-square values, are equal to 1.36 for the MT data and 0.29 for the seismic data. The model is constructed from the predefined crustal 1-D inversion MT and seismic models, which are included as input for the LitMod code. Seismic attenuation and radial anisotropy have been included appropriately in the models. This best-fitting model reproduces both Rayleigh and Love dispersion curves and the MT responses in the Qiangtang area within the associated uncertainties. The average topography (4.8 km) is also reproduced by a 100 km-thick fertile lithosphere with an average crustal density of 2885 kg/m^3 (Table 2) and a Moho depth of 66 km as established from various seismic studies [e.g., *Zhao et al.*, 2001; *Kind et al.*, 2002; *Kumar et al.*, 2006; *Li et al.*, 2006; *Nábělek et al.*, 2009; *Yue et al.*, 2012].

One surface heat flow measurement has been made in the Qiangtang Terrane, but it is far from our study area and is surprisingly low (45 mW/m^2) [*Pollack et al.*, 1993, *Wang*, 2001, *Jiménez-Munt et al.*, 2008]. Our best-fitting model is characterized by a far higher SHF at 80 mW/m^2. Thus, our model does not yield a low SHF, but no model can be found with such a low SHF that is consistent with the other observations.

© 2014. American Geophysical Union. All Rights Reserved.

For comparison, three different models with LAB depths of 80 km (red), 100 km (green), and 120 km (blue) are shown in Figure 5. The best fitting integrated models were obtained for predefined thermal and mechanical parameters of the crust and dry mantle. The study of crustal and mantle parameters ranges of our modeling are presented for the more complex modeling of the Lhasa Terrane below.

6.2. Lhasa Terrane

In the southern part of line 500 (Lhasa Terrane, Figure 1), the thermal lithosphere appears to be thicker than in the Qiangtang Terrane, about 140–220 km based on modeling the surface-wave data alone. For the assigned crustal parameters (Table 2) and a Moho depth of 75 km, we fit the average topography with a SHF of about 77 mW/m^2 (see below for a discussion on the effect of varying the crustal thickness). This SHF is slightly lower than in the Qiangtang Terrane model. However, such a cold and thick lithospheric structure is at odds with long period MT data ($>$1000 s), at least for a dry mantle. The lithospheric mantle is too resistive to explain the MT responses at long periods, regardless of the lithospheric thickness (Figure 6).

There are several factors that can very effectively decrease the electrical resistivity of the mantle (e.g., minor conducting phases, melt or water). Here we test the hypothesis of small amounts of water (hundreds of ppm) in nominally anhydrous minerals (NAMs). Such tiny amounts of water significantly affect mantle resistivity but leave seismic velocities totally unaffected (and therefore, calculated surface-wave dispersion curves would not be affected). The hypothesis of a wet mantle below the Lhasa Block (at least its west-central area) is further inferred by the presence of hydrous minerals (i.e., phlogopite) in some of the Fe-rich harzburgites in xenoliths from Sailipu [*Liu et al*., 2011, Table 1].

Of all of the compositions considered in this study, only composition 4 (phlogopite-bearing Fe-rich spinel harzburgite from West Lhasa) shows evidence of hydrous minerals (Table 1). Given that dry compositions have been excluded by the long-period MT data (Figure 6), we will assume composition 4 from Table 1 as representative of the lithospheric mantle in Lhasa. Unfortunately, the xenoliths from West Lhasa are spinel harzburgites that sample relatively shallow parts of the mantle (depths of 60–80 km). In the absence of direct information about the lithosphere below $\sim$80 km (i.e. within the garnet stability field), we will assume the composition from the hydrous spinel xenoliths in West Lhasa as representative of the whole lithosphere. We note that spinel and garnet compositions from the same xenolith locality, or based on global averages for terranes of the same age, translate into only moderate compositional, density, and seismic velocity changes [e.g., *Griffin et al*. 1999; *Jones et al*., 2014, their Table 9] likely to lie within the uncertainty range of the average topography we are modelling here ($\pm$200 m). Furthermore, the Fe-rich hydrous harzburgites from West Lhasa are associated with densities similar to those related to other average lherzolitic garnet compositions (for instance, composition 1 in Table 1). Other harzburgitic garnet compositions based on global averages (e.g., Archons or Protons according to *Griffin et al*., [1999]) predict an unrealistically buoyant lithosphere impossible to reconcile with the other observables modeled here (topography, SW, SHF, and MT data). The effects of varying the mantle compositions considered in this study (Table 1) are shown in Figure 7a, where the possible variation of the predicted LAB for defined ranges of Moho depths and crustal average density is outlined. Seismic velocities are slightly affected, within experimental error, whereas the changes in the predicted topography are significant (400–900 m variation). It should be noted that mantle compositional effects on the buoyancy of the lithosphere (e.g., average topography) trade off with the assumed crustal thickness and average density (as shown in Figure 7b), where we are presenting the possible variation of the predicted topography for defined ranges of input Moho and LAB depths and crustal average density. Disregarding water, the effect of compositional variation on the synthetic MT responses is negligible.

The effect of water on the electrical conductivity of olivine is computed according to the three proton conduction models mentioned above (Figures 8a and 8b: model 1—*Wang et al*. [2006]; model 2—*Yoshino et al*. [2009]; model 3—*Jones et al*. [2012]). Olivine water content is the dominant parameter (olivine represents 60–85% of total mineral assemblage) and hence, in as much as its value is fixed, the water content in the other mineral phases (and hence the choice of the water partition coefficients) is a second-order parameter. In Appendix A, we demonstrate that the considerable difference in bulk water content based on the different partition coefficients has a minor effect in the predicted MT responses, but potentially has a strong effect on geodynamical properties of lithospheric mantle [*Peslier*, 2010] and should not be neglected. The minor effect of partitioning on the predicted MT responses is caused by the fixed water content of olivine.

© 2014. American Geophysical Union. All Rights Reserved.

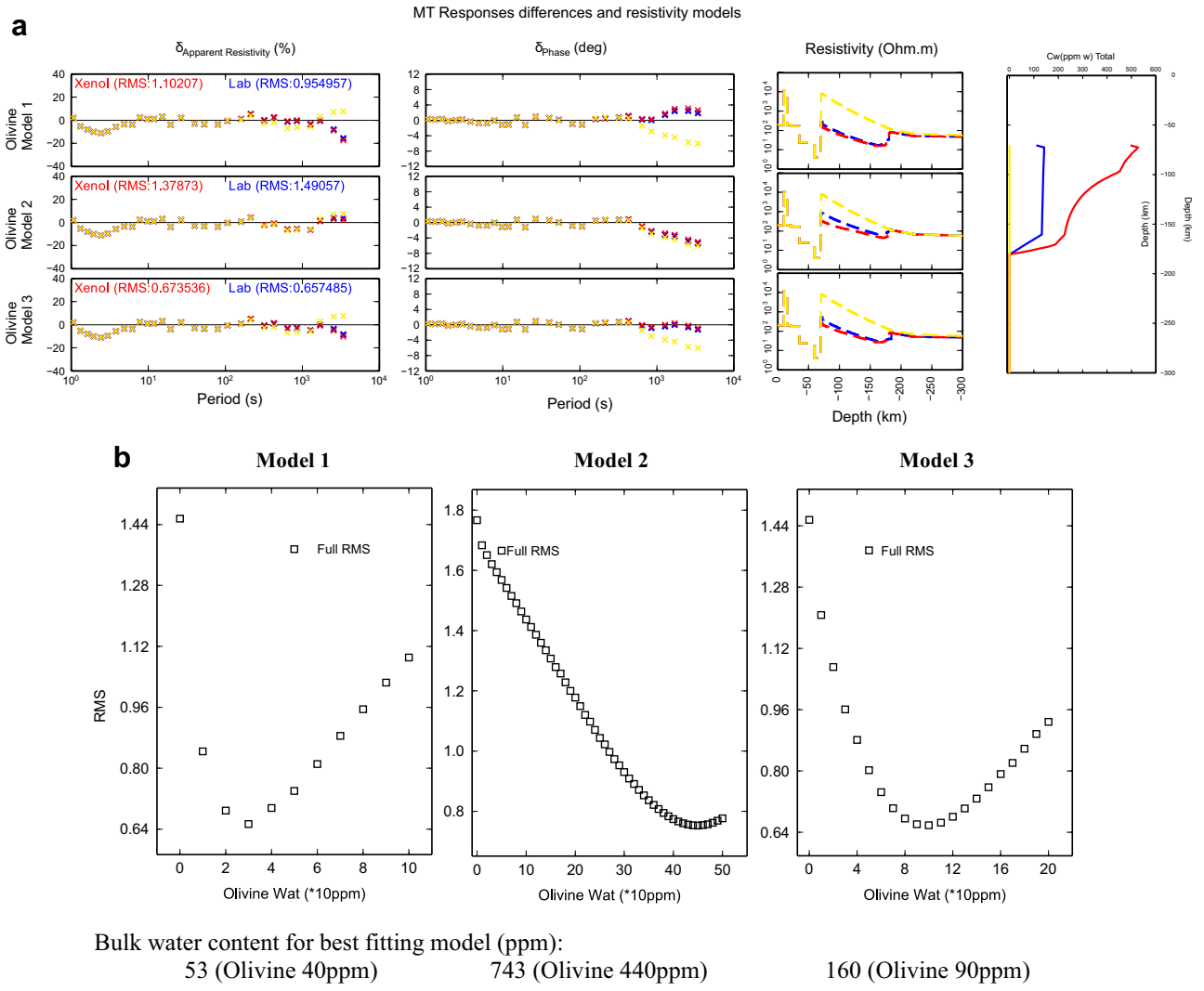

Figure 8. (a) Water content partitioning (red – based on xenolith information, blue – based on laboratory information, and yellow – dry lithosphere models) in rocks and different proton conduction models for fixed 80 ppm olivine water content. (b) Comparison of different proton conduction models (laboratory partitioning). Graphs represent RMS misfit of MT data for different olivine water contents in mantle and derived bulk water content. The olivine (bulk) water content distribution with depth is identical to that presented in Figure 8(a).

The bulk water content for xenolith-based partition coefficients is too high and there is no evidence that such a large concentration of water can be expected in mantle rocks [*Xia et al*., 2010, *Kovács et al*., 2012]. Therefore, laboratory-based partitioning of water (Table 3) is assumed in the rest of the study presented below.

The average amounts of water in olivine required to fit the MT data are 40, 440, and 90 ppm for proton conduction models 1 (Karato), 2 (Yoshino), and 3 (Jones), respectively (Figure 8b). The olivine water content translates into bulk water contents of 53, 743, and 160 ppm respectively for these proton conduction models. The Yoshino model (743 ppm total water content) can be excluded, because the implied bulk water content is far too high for lithospheric mantle rocks; measurements by *Kovács et al*. [2012] imply a maximum water content in lithospheric rocks of 190 wt ppm.

Table 3. Water Partitioning Coefficient Used in the Modeling to Calculate Water Content for Clinopyroxene and Orthopyroxene in the Mantle From Input Value of Olivine Water Content[a]

	Olivine C_w^{ol}	C_w^{ol}/C_w^{opx} Orthophyroxene	C_w^{clp}/C_w^{opx} Clinopyroxene	Garnet (ppm)
Laboratory[b]	Input	0.15	2.5	5
Xenoliths[c]	Input	0.0246	2.1	5

[a]Garnet water content is fixed to 5 ppm.
[b]Laboratory results for partitioning [*Aubaud et al*. 2004; *Kovacs et al*. 2012].
[c]Partitioning coefficient based on xenolith samples [*Grant et al*., 2007].

© 2014. American Geophysical Union. All Rights Reserved.

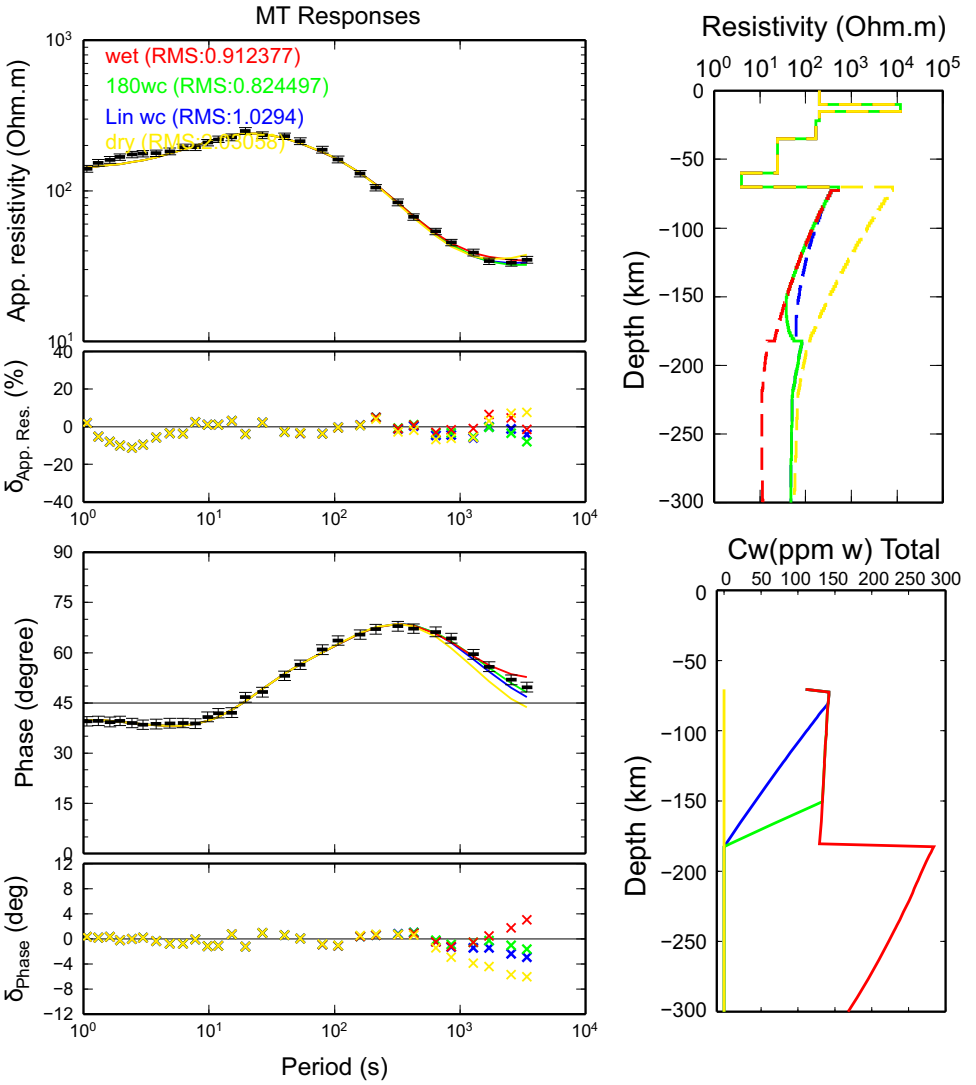

Figure 9. Wet Lhasa modeling for three different water distributions within mantle: blue—linear decrease from 80 km to LAB depth 180 km, green—linear decrease from 160 km to 180 km, red—full wet mantle, and yellow—dry mantle.

In terms of the vertical distribution of water for all models above, the base of the wet layer, which extends from the base of the crust, roughly coincides with the base of the thermal lithosphere in our models (160–180 km) (Figure 9). The presence of water, driven by olivine water content, in the lithospheric mantle (green line in Figure 9) is constant from the Moho to 160 km and then decreases to the LAB depth at 180 km [*Peslier et al.*, 2010]. This vertical water distribution is compared with a completely wet mantle and linear decrease of water content from about the Moho depth to dry values at the LAB depth in order to demonstrate the sensitivity of MT responses to different vertical water distributions. For linearly decreasing olivine water content from the Moho down to 160 km, the lithospheric mantle becomes too resistive. For a fully wet mantle with constant water content with depth, the models are too conductive to fit the MT data.

Our results for the Lhasa Block favor a wet mantle with the presence of water in the underthrusting Indian lithosphere (i.e. above 180 km depth), probably as a result of dehydration processes. We interpret the thick lithosphere under Lhasa as a result of the underthrusting of a relatively warm (at least compared to eastern Lhasa, see *Agius and Lebedev*, [2013]) and wet Indian lithosphere beneath Tibet, where the lithospheric mantle would have undergone metasomatism (e.g., Fe-enrichment of a previously depleted mantle, and rehydration).

© 2014. American Geophysical Union. All Rights Reserved.

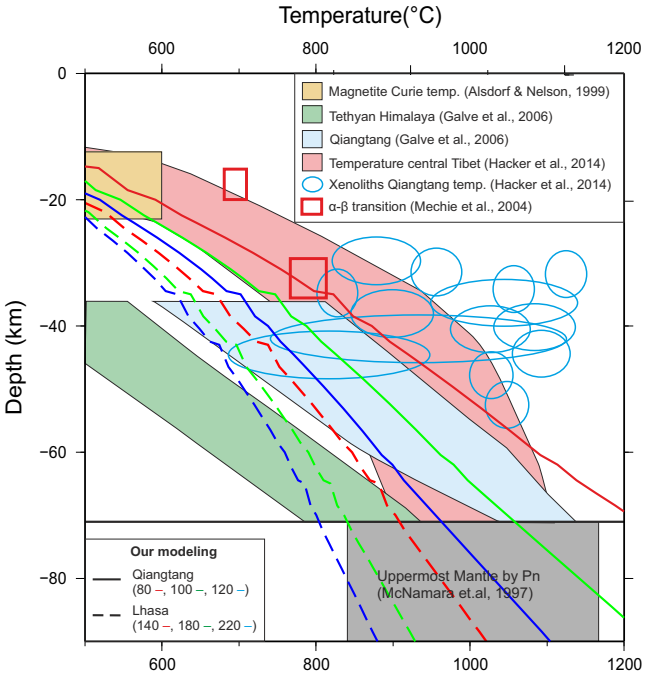

Figure 10. Temperature in depth from calculated models compared with known data [*Mechie et al.*, 2004—red squares; *Galve et al.*, 2006 blue and green areas; *Hacker et al.*, 2014 purple area and blue empty ellipses]. Thin solid lines represent our modeling results for the temperature distribution in Qiangtang for the LAB: red 80-km, green-100 km, blue-120 km. The dashed lines indicate Lhasa temperatures (red-140 km, green-180 km, and blue-220 km).

7. Discussion

The LitMod modeling approach, working within a self-consistent petrological-geophysical thermodynamic framework where mantle properties are calculated as a function of temperature, pressure, and composition, puts new constraints on models of the lithospheric mantle in central Tibet by fitting different geophysical observables and topography. Long-period surface-wave phase velocities are most sensitive to seismic wave speeds and, through them, to temperature within the lithosphere and sublithospheric mantle. They are only weakly sensitive to small amounts of water, i.e. 1 wt% (i.e., 10,000 ppm) water reduces seismic velocity by only 1% [*Karato*, 2006; *Karato*, 2011]. Surface topography is sensitive to the density distribution in the crust and upper mantle, the latter being affected by the geotherm and bulk composition. The electrical conductivity of the mantle is sensitive to temperature and water content distribution [*Jones et al.*, 2009]. Our modeling has integrated quantitatively the complementary sensitivities of the different data types.

In our modeling, a steady state thermal environment was assumed and the temperature distribution was calculated by LitMod based on the thermal conductivity and radiogenic heat production coefficients in the crust and mantle (Figure 10), and thicknesses of the crust and lithospheric mantle [*Fullea et al.*, 2009]. The observed temperature distribution with depth in the Qiangtang Block is lower than the ~700°C inferred at a depth of 18 km by α-β quartz transition [*Mechie et al.*, 2004] and is in agreement with Qiangtang crustal temperature ranges predicted by seismic velocities [*Galvé et al.*, 2006]. The radioactive heat generation in thickened crust contributes to an increase in middle and lower crustal temperatures, where melting can occur for temperatures exceeding the solidus curve. The earthquakes presented in Figure 3 exhibit quite a uniform distribution in the whole crust in the area of line 500. The Lhasa Block modeling exhibits colder thermal conditions that are different from other central Tibetan thermal studies [*Hacker et al.*, 2014], with the lower crustal temperatures similar to those of the Greater Himalaya [*Galvé et al.*, 2006]. The MT models of our Lhasa target area exhibit highly electrically conductive structures near the very base of the crust only, with the middle and upper crust remaining resistive. This suggests a difference in thermal conditions between the lower crust and the middle/upper crust and the lack of melt beneath Lhasa target area.

The results of our integrated geophysical-petrological modeling support the underthrusting of the Indian lithospheric mantle beneath the Lhasa Block, as has been observed in seismic studies [*Tilmann et al.*, 2003;

© 2014. American Geophysical Union. All Rights Reserved.

Kind and Yuan, 2010, *Nunn et al*., 2013]. The presence of hot, melted rocks at sub-Moho depths is not required to fit the MT and seismic data, which suggests that there is no asthenospheric material between the Tibetan crust and the Indian mantle lithosphere for a latitude of $\sim 31^{\circ}$. In this respect, our results do not support the model of the subduction of Indian lithospheric mantle as presented by in *Chen and Özalaybey* [1998] and the central line of *Zhao et al*. [2011]. Our results are broadly consistent with the results of seismic tomography, showing high velocities beneath the Moho in southern Tibet and low velocities in central and northern Tibet [e.g., *Barazangi and Ni*, 1982; *Brandon and Romanowicz*, 1986; *Bourjot and Romanowicz*, 1992; *Li et al*., 2008a; *Priestley et al*., 2008; *Schaeffer and Lebedev*, 2013; *Agius and Lebedev*, 2013]. However, our thermodynamic modeling approach provides a far more robust and accurate estimate of the depth of the lithosphere-asthenosphere boundary than seismic or MT inversions alone.

The dry Tibetan Qiangtang lithosphere implies that there are no hydration processes below it leading to metasomatism. Due to the poor penetration of Qiangtang MT data, we cannot extend our models to depths below the Tibetan sublithosphere ($z > 150$ km). Therefore, the presence of Indian lithospheric mantle at depths greater than 150 km beneath the Qiangtang Terrane cannot be investigated with our data.

There has been broad discussion regarding the depths of earthquakes in the Tibetan region with important implications for temperature parameters and water content in the crust and lithospheric mantle [*Jackson*, 2002; *Priestley et al*., 2008; *Searle et al*., 2011]. The lack of deep earthquakes is likely to be related in some manner to the amount of water in the lithospheric mantle [*Maggi et al*., 2000], with the water reducing the strength and viscosity of the mantle [*Jackson*, 2002; *Lee et al*., 2011]. However, the occurrence of earthquakes at sub-Moho depths south of our area of investigation [*Chen and Yang*, 2004; *Monsalve et al*., 2006] favors the idea that there are localized areas where the continental upper mantle deforms by brittle processes. There is a simpler explanation for aseismic deep structures based on temperature, where the earthquakes occur in mantle colder than 600°C [*McKenzie et al*., 2005]. The effect of a small amount of water on seismic velocities is insignificant [*Karato*, 2011], and the seismic velocities are not affected by water content in this study from the LitMod model design. Due to the lack of deep mantle xenolith samples from central Tibet, we have no other lines of evidence to support the water content values. However, water is proving to be a common component of cratonic lithospheres at levels of tens to low hundreds of wt ppm [*Li et al*., 2008b; *Peslier*, 2010; *Doucet et al*., 2014]. We modeled a distribution of water where dry olivine is placed at the bottom of the Indian lithosphere, consistent with the observations of *Peslier et al*. [2010] for the Kaapvaal Craton. The effect of this water content distribution ($<$0.02 wt%) on the seismic surface phase velocities is insignificant in comparison with dry lithosphere, but significant for the deformation and evolution of the continent-continent collision [*Karato*, 2010].

Recent seismic data and models from central Tibet [*Liang et al*., 2012; *Ceylan et al*., 2012; *Nunn et al*., 2013] bring new complexity to the mantle modeling of central Tibet. The 1-D integrated models presented here, based on lateral averages, represent a useful starting step to define a reliable 3-D physical, geodynamic, and compositional model of the area. The presented integrated modeling provides a robust averaged image of the region, which covers an area of several degrees in longitudinal and latitudinal direction around the INDEPTH 500 line constrained by different and complementary data sets.

The comparison of different proton conduction models used to test the water content partitioning in minerals shows a difference in bulk water content over a factor of 10 (see Figure 8b). Further laboratory experiments are needed to reconcile their differences. The disparity in the laboratory observations favors laboratory studies calibrated with geophysical observations [*Jones et al*., 2012]. The use of the *Yoshino et al*. [2009] model, with low-conductive effects of water, results in far too high a bulk water content for real mantle rocks [*Kovács et al*., 2012] to fit the MT data and we can exclude it. In all probability, the most important parameter for the conductivity of the modeled mantle is olivine water content. This study shows how water partitioning in minerals is of relatively low importance for the conductivity of mantle rock assemblages.

The MT data from INDEPTH line 500 alone were used to model in 1-D selected magnetotelluric transfer functions which exhibit high penetration depths. The presence of partial melt in lower crustal structures is inferred by a strong conductor below the northern part of the Lhasa Terrane and mid-to-lower crustal conductors in the southern part of the Qiangtang Terrane. Also, the MT-only inversions are insensitive to very resistive upper parts of the lithospheric mantle directly below the Moho, because these are "hidden" by conductive crustal structures [see, e.g., Figure 3 in *Jones*, 1999]. For the Lhasa Terrane group, the models

© 2014. American Geophysical Union. All Rights Reserved.

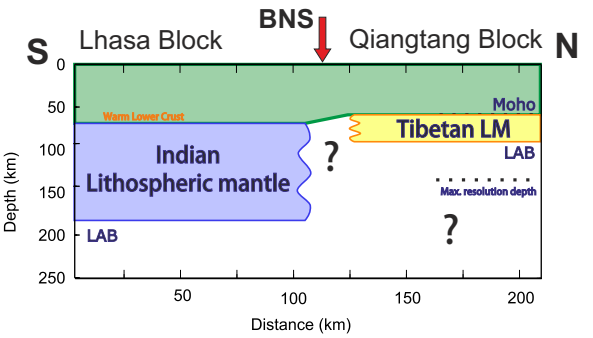

Figure 11. Cartoon showing the tectonic situation in central Tibet based on the petrological-geophysical modeling presented in this study.

show the existence of a high-conductivity layer located at a depth greater than 200 km, whereas for the Qiangtang Terrane this conductive layer appears to be located at a depth of less than 180 km. The changes between the averaged 1-D models and the nonuniqueness of models fitting the data within the error bars are the most likely reason for deeper MT LAB estimation (section 5.1) in comparison with the integrated models presented here. In our modeling, we have used fixed isotropic conductivity and seismic velocity parameters for the crust from independent MT 1-D and surface-waves phase-velocity inversions. All possible effects of crustal partial melt or fluids on geophysical observables are included in this primary input. We do not take into account the existence of partial melt in the lithospheric mantle for this simplified 1-D integrated study (i.e., the data can be explained without this hypothesis).

8. Conclusions

1-D integrated petrological-geophysical modeling was performed for two groups of sites; the first group in the northern part of the Lhasa Terrane (southern part of INDEPTH line 500) and the second group in the southern part of the Qiangtang Terrane (northern part of line 500). Final 1-D models suggest a LAB depth of 80–120 km of dry lithosphere in the Qiangtang Terrane. In the Lhasa Terrane, the LAB depth is about 180 km according to surface waves and topography. In comparison with MT-only modeling as described above, the lithospheric thickness is less. We consider the results of integrated modeling constrained with more geophysical observables as a far more robust estimation. The presence of small amounts of water in the lithospheric mantle ($<$0.02 wt%) is required to fit the magnetotelluric responses for the Lhasa Terrane, but in contrast the Qiangtang Terrane can be explained by dry mineral assemblages without resorting to the inclusion of an additional conducting component. The mantle composition in the Lhasa Terrane is compatible with a phlogopite-bearing Fe-rich spinel harzburgitic composition based on xenolith data from West Lhasa, suggesting metasomatism (e.g. Fe-enrichment of a previously depleted mantle, and rehydration as evidenced by the hydrous mineral phases). In contrast, the composition modeled in the Qiangtang Terrane corresponds to a relatively fertile and dry composition (garnet lherzolite), as commonly present in Asian mantle xenolith data (see Table 1). The modeling also implies low-angle subduction or underthrusting and does not indicate downwelling of the Indian lithosphere below the Lhasa Terrane, because of the inference of the existence of underlying asthenosphere.

The integrated petrological modeling suggests that south of the BNS the Tibetan Plateau consists of thick crust and thick, compact, non-cratonic Indian lithospheric-mantle with a small amount of water (Figure 11). The Tibetan Plateau north of the BNS is underlain by a thinner crust and thin, hot, dry Tibetan lithospheric mantle. The lack of MT data penetration in our integrated modeling leaves hypotheses of the existence of Indian lithosphere north of the BNS still open.

Appendix A

In principle, water can be differently distributed in any of the uppermost mantle minerals, so it is important to define the water partitioning between them (e.g. C_w^{ol}/C_w^{opx} or C_w^{clp}/C_w^{opx}, where C_w^{ol}, C_w^{clp}, and C_w^{opx} are the water contents in olivine, clinopyroxene, and orthopyroxene, respectively). Measurements made on mantle xenoliths and laboratory studies show a range of partition coefficients. *Peslier et al*. [2010] and *Baptiste et al*. [2012] both show very strong depth variations for water in olivine for the Kaapvaal Craton with maximum water content in the middle of the lithosphere at 100–120 km (of order 100 wt ppm) reducing to virtually dry (10 wt ppm) at the base of the lithosphere at 200 km, but the water content in the pyroxenes, both orthopyroxene and clinopyroxene appear to be depth-independent. These field observations imply that

© 2014. American Geophysical Union. All Rights Reserved.

there is either no water partition coefficient between olivine and the pyroxenes, or that the water partitioning is depth-dependent, consistent with the observations of *Férot and Bolfan-Casanova*, [2012]. In contrast, recent results for the Siberian Craton show depth-independent water content in olivine with partitioning between olivine and clinopyroxene [*Doucet et al*., 2013].

Here, two end-member water partition coefficient models are assumed, based on xenolith [*Grant et al*., 2007] and laboratory studies [*Aubaud et al*., 2004; *Tenner et al*., 2009; *Inoue et al*., 2010; *Kovács et al*., 2012] (Table 3). In order to simplify our models, and given the modal abundances (i.e., olivine represents 60–90% of total mineral assemblage [*Ding et al*., 2007]), we consider the amount of olivine as a free model parameter and compute the bulk, whole-rock amount of water based on the above-mentioned water partition coefficients as well as the modal distribution of the minerals, keeping in mind the restrictions associated with the solubility of water in the different minerals [e.g. *Fullea et al*., 2011]. Water content in garnet is assumed to be negligible, as garnet shows very little water in mantle xenoliths [*Peslier*, 2010]. The effect of water on the electrical conductivity of olivine is computed according to the three proton conduction models mentioned above (Figures 8a and 8b: model 1—*Wang et al*. [2006]; model 2—*Yoshino et al*. [2009]; and model 3—*Jones et al*. [2012]).

The effect of the different water partition coefficients (Table 3) for the different olivine proton conduction models (1–3) is shown in Figure 8a. The average bulk water content in the lithosphere (for fixed olivine water content of 80 ppm) varies from around 526 ppm, assuming xenolith-based partition coefficients, to 141 ppm when the partition coefficients are based on laboratory studies (Table 3).

Acknowledgments

We would like to thank two anonymous reviewers, Associate Editor Barbara Romanowicz and Editor-in-Chief Thorsten Becker for detailed, constructive comments that helped us to improve the manuscript. We thank Science Foundation of Ireland (SFI) for the financial support of grants 08/RFP/GEO1693 "INDEPTH4," 10/IN.1/I3022 "IRETHERM," and the members of the INDEPTH MT team from China, U.S.A., Canada and Ireland. Javier Fullea was supported by the JAE-DOC programme (CSIC-Spain) cofounded by ESF, and by Spanish Ministry of Economy and Competitiveness grant CGL2012-37222. M.R.A. and S.L. acknowledge support, at early stages of this work, from SFI (grants 08/RFP/GEO1704 and 09/RFP/GEO2550). The MT component of Project INDEPTH has been supported by the Ministry of Land and Natural Resources of China and the U.S. National Science Foundation's Continental Dynamics Program.

References

Afonso, J. C., and S. Zlotnik (2011), The subductability of continental lithosphere: The before and after story, in *Arc-Continent Collision, Frontiers in Earth Sciences*, edited by D. Brown and P. D. Ryan, pp. 53–86, Springer, Berlin Heidelberg.

Afonso, J. C., G. Ranalli, and M. Fernàndez (2005), Thermal expansivity and elastic properties of the lithospheric mantle: Results from mineral physics of composites, *Phys. Earth Planet. Inter.*, *149*(3-4), 279–306, doi:10.1016/j.pepi.2004.10.003.

Afonso, J. C., M. Fernàndez, G. Ranalli, W. L. Griffin, and J. A. D. Connolly (2008), Integrated geophysical-petrological modeling of the lithosphere and sublithospheric upper mantle: Methodology and applications, *Geochem. Geophys. Geosyst.*, *9*, Q05008, doi:10.1029/2007GC001834.

Afonso, J. C., G. Ranalli, M. Fernàndez, W. L. Griffin, S. Y. O'Reilly, and U. H. Faul (2010), On the Vp/Vs–Mg# correlation in mantle peridotites: Implications for the identification of thermal and compositional anomalies in the upper mantle, *Earth Planet. Sci. Lett.*, *289*(3-4), 606–618, doi:10.1016/j.epsl.2009.12.005.

Agius, M. R., and S. Lebedev (2013), Tibetan and Indian lithospheres in the upper mantle beneath Tibet: Evidence from broadband surface-wave dispersion, *Geochem. Geophys. Geosyst.*, *14*, 4260–4281, doi:10.1002/ggge.20274.

Allègre, C. J., et al. (1984), Structure and evolution of the Himalaya–Tibet orogenic belt, *Nature*, *307*, 17–22.

Argand, E. (1924), La tectonique de l'Asie, *Extr. du Compte-rendu du XIIIe Congrès géologique Int. Liège*, *1*, 171–372.

Aubaud, C., E. H. Hauri, and M. M. Hirschmann (2004), Hydrogen partition coefficients between nominally anhydrous minerals and basaltic melts, *Geophys. Res. Lett.*, *31*, L20611, doi:10.1029/2004GL021341.

Bai, D., et al. (2010), Crustal deformation of the eastern Tibetan plateau revealed by magnetotelluric imaging, *Nat. Geosci.*, *3*(5), 358–362, doi:10.1038/ngeo830.

Bai, Z., S. Zhang, and C. Braitenberg (2013), Crustal density structure from 3D gravity modeling beneath Himalaya and Lhasa blocks, Tibet, *J. Asian Earth Sci.*, *78*, 301–317, doi:10.1016/j.jseaes.2012.12.035.

Baptiste, V., A. Tommasi, and S. Demouchy (2012), Deformation and hydration of the lithospheric mantle beneath the Kaapvaal craton, South Africa, *Lithos*, *149*, 31–50, doi:10.1016/j.lithos.2012.05.001.

Barazangi, M., and J. Ni (1982), Velocities and propagation characteristics of Pn and Sn beneath the Himalayan arc and Tibetan plateau: Possible evidence for underthrusting of Indian continental, *Geology*, *10*, 179–185.

Barron, J., and K. Priestley (2009), Observations of frequency-dependent S n propagation in Northern Tibet, *Geophys. J. Int.*, *179*(1), 475–488, doi:10.1111/j.1365-246X.2009.04318.x.

Barry, T. L., A. D. Saunders, P. D. Kempton, B. F. Windley, M. S. Pringle, D. Dorjnamjaa, and S. Saandar (2003), Petrogenesis of Cenozoic basalts from Mongolia: Evidence for the role of asthenospheric versus metasomatized lithospheric mantle sources, *J. Petrol.*, *44*(1), 55–91.

Berdichevsky, M. N., and V. I. Dmitriev (2008), *Models and Methods of Magnetotellurics*, Springer, Berlin, Heidelberg.

Bird, P. (1991), Lateral extrusion of lower crust from under high topography in the isostatic limit, *J. Geophys. Res.*, *96*(B6), 10,275–10,286.

Bourjot, L., and B. Romanowicz (1992), Crust and uppermantle tomography in Tibet using surface waves, *Geophys. Res. Lett.*, *19*(9), 881–884.

Brandon, C., and B. Romanowicz (1986), A "no-lid" zone in the central Chang-Thang platform of Tibet: Evidence from pure path phase velocity measurements of long period Rayleigh waves, *J. Geophys. Res.*, *91*(B6), 6547–6564.

Cammarano, F., S. Goes, P. Vacher, and D. Giardini (2003), Inferring upper-mantle temperatures from seismic velocities, *Phys. Earth Planet. Inter.*, *138*(3-4), 197–222, doi:10.1016/S0031-9201(03)00156-0.

Ceylan, S., J. Ni, J. Y. Chen, Q. Zhang, F. Tilmann, and E. Sandvol (2012), Fragmented Indian plate and vertically coherent deformation beneath eastern Tibet, *J. Geophys. Res.*, *117*, B11303, doi:10.1029/2012JB009210.

Chen, L., J. R. Booker, A. G. Jones, N. Wu, and M. J. Unsworth (1996), Electrically conductive crust in southern Tibet from INDEPTH magnetotelluric surveying, *Science*, *274*, 1694–1696.

Chen, W.-P., and S. Özalaybey (1998), Correlation between seismic anisotropy and Bouguer gravity anomalies in Tibet and its implications for lithospheric structures, *Geophys. J. Int.*, *135*(1), 93–101, doi:10.1046/j.1365-246X.1998.00611.x.

© 2014. American Geophysical Union. All Rights Reserved.

Chen, W.-P., and Z. Yang (2004), Earthquakes beneath the Himalayas and Tibet: Evidence for strong lithospheric mantle., *Science*, *304*(5679), 1949–52, doi:10.1126/science.1097324.
Christensen, N. I., and W. D. Mooney (1995), Seismic velocity structure and composition of the continental crust: A global view, *J. Geophys. Res.*, *100*(B7), 9761–9788.
Clark, M. K., and L. H. Royden (2000), Topographic ooze: Building the eastern margin of Tibet by lower crustal flow, *Geology*, *28*, 703–706, doi:10.1130/0091-7613(2000)28<703.
Connolly, J. A. D. (2005), Computation of phase equilibria by linear programming: A tool for geodynamic modeling and its application to subduction zone decarbonation, *Earth Planet. Sci. Lett.*, *236*, 524–541, doi:10.1016/j.epsl.2005.04.033.
Connolly, J. A. D., and D. M. Kerrick (2002), Metamorphic controls on seismic velocity of subducted oceanic crust at 100–250 km depth, *Earth Planet. Sci. Lett.*, *204*(1-2), 61–74, doi:10.1016/S0012-821X(02)00957-3.
Constable, S. C., R. L. Parker, and C. G. Constable (1987), Smoothing, splines and smoothing splines: Their application in geomagnetism, *Geophysics*, *52*(3), 289–300, doi:10.1016/0021-9991(88)90062-9.
Dai, L., and S. Karato (2009), Electrical conductivity of orthopyroxene: Implications for the water content of the asthenosphere, *Proc. Jpn. Acad. Ser. B*, *85*(10), 466–475, doi:10.2183/pjab.85.466.
Dewey, J. F., and J. M. Bird (1970), Mountain belts and the new global tectonics, *J. Geophys. Res.*, *75*(14), 2625–2647.
Dewey, J. F., R. M. Shackleton, C. Chengfa, and S. Yiyin (1988), The Tectonic Evolution of the Tibetan Plateau, *Philos. Trans. R. Soc. London A*, *327*(1594), 379–413, doi:10.1098/rsta.1988.0135.
Ding, L., P. Kapp, Y. Yue, and Q. Lai (2007), Postcollisional calc-alkaline lavas and xenoliths from the southern Qiangtang terrane, central Tibet, *Earth Planet. Sci. Lett.*, *254*(1-2), 28–38, doi:10.1016/j.epsl.2006.11.019.
Doucet, L. S., A. H. Peslier, D. A. Ionov, and A. D. Brandon (2013), High water contents in the Siberian cratonic mantle: An FTIR study of Udachnaya peridotite xenoliths, Abstract T23A-2563 presented at 2013 AGU Fall Meeting, AGU, San Francisco, Calif.
Doucet, L. S., A. H. Peslier, D. A. Ionov, A. D. Brandon, A. V. Golovin, A. G. Goncharov, and I. V. Ashchepkov (2014), High water contents in the Siberian cratonic mantle linked to metasomatism: An FTIR study of Udachnaya peridotite xenoliths, *Geochim. Cosmochim. Acta*, *137*, 159–187, doi:10.1016/j.gca.2014.04.011.
Eaton, D. W., F. Darbyshire, R. L. Evans, H. Grütter, A. G. Jones, and X. Yuan (2009), The elusive lithosphere–asthenosphere boundary (LAB) beneath cratons, *Lithos*, *109*(1-2), 1–22, doi:10.1016/j.lithos.2008.05.009.
Faul, U. H., and I. Jackson (2005), The seismological signature of temperature and grain size variations in the upper mantle, *Earth Planet. Sci. Lett.*, *234*, 119–134, doi:10.1029/2001JB001225.
Férot, A., and N. Bolfan-Casanova (2012), Water storage capacity in olivine and pyroxene to 14GPa: Implications for the water content of the Earth's upper mantle and nature of seismic discontinuities, *Earth Planet. Sci. Lett.*, *349–350*, 218–230, doi:10.1016/j.epsl.2012.06.022.
Francheteau, J., C. Jaupart, S. X. Jie, K. Wen-Hua, L. De-Lu, B. Jia-Chi, W. Hung-Pin, and D. Hsia-Yeu (1984), High heat flow in southern Tibet, *Nature*, *307*, 32–36.
Fullea, J., J. C. Afonso, J. A. D. Connolly, M. Fernàndez, D. García-Castellanos, and H. Zeyen (2009), LitMod3D: An interactive 3-D software to model the thermal, compositional, density, seismological, and rheological structure of the lithosphere and sublithospheric upper mantle, *Geochem., Geophys. Geosyst.*, *10*, Q08019, doi:10.1029/2009GC002391.
Fullea, J., M. R. Muller, and A. G. Jones (2011), Electrical conductivity of continental lithospheric mantle from integrated geophysical and petrological modeling: Application to the Kaapvaal Craton and Rehoboth Terrane, southern Africa, *J. Geophys. Res.*, *116*, B10202, doi:10.1029/2011JB008544.
Fullea, J., S. Lebedev, M. R. Agius, A. G. Jones, and J. C. Afonso (2012), Lithospheric structure in the Baikal-central Mongolia region from integrated geophysical-petrological inversion of surface-wave data and topographic elevation, *Geochem. Geophys. Geosyst.*, *13*, Q0AK09, doi:10.1029/2012GC004138.
Fullea, J., M. R. Muller, A. G. Jones, and J. C. Afonso (2014), The lithosphere–asthenosphere system beneath Ireland from integrated geophysical–petrological modeling II: 3D thermal and compositional structure, *Lithos*, *189*, 49–64, doi:10.1016/j.lithos.2013.09.014.
Galvé, A., M. Jiang, A. Hirn, M. Sapin, M. Laigle, B. de Voogd, J. Gallart, and H. Qian (2006), Explosion seismic P and S velocity and attenuation constraints on the lower crust of the North–Central Tibetan Plateau, and comparison with the Tethyan Himalayas: Implications on composition, mineralogy, temperature, and tectonic evolution, *Tectonophysics*, *412*(3-4), 141–157, doi:10.1016/j.tecto.2005.09.010.
Gan, W., P. Zhang, Z.-K. Shen, Z. Niu, M. Wang, Y. Wan, D. Zhou, and J. Cheng (2007), Present-day crustal motion within the Tibetan Plateau inferred from GPS measurements, *J. Geophys. Res.*, *112*, B08416, doi:10.1029/2005JB004120.
Gao, R., Z. Lu, Q. Li, Y. Guan, J. Zhang, R. He, and L. Huang (2005), Geophysical survey and geodynamic study of crust and upper mantle in the Qinghai-Tibet Plateau, *Episodes*, *28*(4), 263–273.
Girardeau, J., J. Marcoux, C. Allegre, J. P. Bassoullet, T. Youking, X. Xuchang, Z. Yougong, and W. Xibin (1984), Tectonic environment and geodynamic significance of the Neo-Cimmerian Donqiao ophiolite, Bangong-Nujiang suture zone, Tibet, *Nature*, *307*, 27–31.
Grant, K., J. Ingrin, J. P. Lorand, and P. Dumas (2007), Water partitioning between mantle minerals from peridotite xenoliths, *Contrib. Mineral. Petrol.*, *154*(1), 15–34, doi:10.1007/s00410-006-0177-1.
Griffin, W. L., S. Y. O'Reilly, and C. G. Ryan (1999), The composition and origin of sub-continental lithospheric mantle, in *Mantle Petrology: Field Observations and High-Pressure Experimentation: A Tribute to Francis R. (Joe) Boyd*, edited by Y. Fei, C. M. Berkta, and B. O. Mysen, *Spec. Publ. Geochem. Soc.*, *6*, 13–45.
Groom, R., and R. Bailey (1989), Decomposition of magnetotelluric impedance tensors in the presence of local three-dimensional galvanic distortion, *J. Geophys. Res.*, *94*, 1913–1925.
Hacker, B. R., M. H. Ritzwoller, and J. Xie (2014), Central tibet has a partially melted, mica-bearing crust, *Tectonics*, *33*, 1408–1424, doi:10.1002/2014TC003545.
Haines, S. S., S. L. Klemperer, L. Brown, G. Jingru, J. Mechie, R. Meissner, A. Ross, and Z. Wenjin (2003), INDEPTH III seismic data: From surface observations to deep crustal processes in Tibet, *Tectonics*, *22*(1), 1001, doi:10.1029/2001TC001305.
Hetényi, G., R. Cattin, F. Brunet, L. Bollinger, J. Vergne, J. L. Nábělek, and M. Diament (2007), Density distribution of the India plate beneath the Tibetan plateau: Geophysical and petrological constraints on the kinetics of lower-crustal eclogitization, *Earth Planet. Sci. Lett.*, *264*(1-2), 226–244, doi:10.1016/j.epsl.2007.09.036.
Holland, T. J. B., and R. Powell (1998), An internally consistent thermodynamic data set for phases of petrological interest, *J. Metamorph. Geol.*, *16*, 309–343.
Houseman, G. A., and P. C. England (1986), Finite strain calculations of continental deformation: 1. Method and general results for convergent zones, *J. Geophys. Res.*, *91*(B3), 3651–3663.
Houseman, G. A., and D. McKenzie (1981), Convective instability of a thickened boundary layer and its relevance for the thermal evolution of continental convergent belts, *J. Geophys. Res.*, *86*(B7), 6115–6132.

© 2014. American Geophysical Union. All Rights Reserved.

Huang, J., and D. Zhao (2006), High-resolution mantle tomography of China and surrounding regions, *J. Geophys. Res.*, *111*, B09305, doi:10.1029/2005JB004066.
Inoue, T., T. Wada, R. Sasaki, and H. Yurimoto (2010), Water partitioning in the Earth's mantle, *Phys. Earth Planet. Inter.*, *183*(1-2), 245–251, doi:10.1016/j.pepi.2010.08.003.
Ionov, D. A. (2002), Mantle structure and rifting processes in the Baikal–Mongolia region: Geophysical data and evidence from xenoliths in volcanic rocks, *Tectonophysics*, *351*(1-2), 41–60, doi:10.1016/S0040-1951(02)00124-5.
International Seismological Centre (2012), *Bulletin of the International Seismological Centre*. [Available at http://www.isc.ac.uk.]
Jackson, J. (2002), Strength of the continental lithosphere: Time to abandon the jelly sandwich?, *GSA Today*, *12*, 4–10.
Jaupart, C., J. Francheteau, and X.-J. Shen (1985), On the thermal structure of the southern Tibetan crust, *Geophys. J. R. Astron. Soc.*, *81*, 131–155, doi:10.1111/j.1365-246X.1985.tb01355.x.
Jaupart, C., S. Labrosse, and J.-C. Mareschal (2007), Temperatures, heat and energy in the mantle of the Earth, *Treatise on Geophysics*, Mantle Dynamics, vol. 7, edited by D. Bercovici and G. Schubert, pp. 253–303, Elsevier, Amsterdam.
Jiménez-Munt, I., and J. P. Platt (2006), Influence of mantle dynamics on the topographic evolution of the Tibetan Plateau: Results from numerical modeling, *Tectonics*, *25*, TC6002, doi:10.1029/2006TC001963.
Jiménez-Munt, I., M. Fernandez, J. Vergés, and J. P. Platt (2008), Lithosphere structure underneath the Tibetan Plateau inferred from elevation, gravity and geoid anomalies, *Earth Planet. Sci. Lett.*, *267*(1-2), 276–289, doi:10.1016/j.epsl.2007.11.045.
Jones, A. G. (1983), On the equivalence of the "Niblett" and "Bostick" transformations in the magnetotelluric method, *J. Geophys.*, *53*, 72–73.
Jones, A. G. (1999), Imaging the continental upper mantle using electromagnetic methods, *Lithos*, *48*(1-4), 57–80, doi:10.1016/S0024–4937(99)00022-5.
Jones, A. G. (2012), Distortion decomposition of the magnetotelluric impedance tensors from a one-dimensional anisotropic Earth, *Geophys. J. Int.*, *189*(1), 268–284, doi:10.1111/j.1365-246X.2012.05362.x.
Jones, A. G. (2014), Compensation of the Meyer-Neldel compensation law for H diffusion in minerals, *Geochem. Geophys. Geosyst.*, *15*, 2616–2631, doi:10.1002/2014GC005261.
Jones, A. G., R. L. Evans, and D. W. Eaton (2009), Velocity–conductivity relationships for mantle mineral assemblages in Archean cratonic lithosphere based on a review of laboratory data and Hashin–Shtrikman extremal bounds, *Lithos*, *109*, 131–143, doi:10.1016/j.lithos.2008.10.014.
Jones, A. G., J. Fullea, R. L. Evans, and M. R. Muller (2012), Water in cratonic lithosphere: Calibrating laboratory-determined models of electrical conductivity of mantle minerals using geophysical and petrological observations, *Geochem. Geophys. Geosyst.*, *13*, Q06010, doi:10.1029/2012GC004055.
Jones, A. G., J. C. Afonso, J. Fullea, and F. Salajegheh (2014), The lithosphere–asthenosphere system beneath Ireland from integrated geophysical–petrological modeling—I: Observations, 1D and 2D hypothesis testing and modeling, *Lithos*, *189*, 28–48, doi:10.1016/j.lithos.2013.10.033.
Kapp, P., A. Yin, T. M. Harrison, and L. Ding (2005), Cretaceous-Tertiary shortening, basin development, and volcanism in central Tibet, *Geol. Soc. Am. Bull.*, *117*(7), 865–878, doi:10.1130/B25595.1.
Karato, S. (1993), Importance of anelasticity in the interpretation of seismic tomography, *Geophys. Res. Lett.*, *20*(15), 1623–1626.
Karato, S. (2006), Remote Sensing of Hydrogen in Earth's Mantle, *Rev. Mineral. Geochem.*, *62*(1), 343–375, doi:10.2138/rmg.2006.62.15.
Karato, S. (2010), Rheology of the deep upper mantle and its implications for the preservation of the continental roots: A review, *Tectonophysics*, *481*(1-4), 82–98, doi:10.1016/j.tecto.2009.04.011.
Karato, S. (2011), Water distribution across the mantle transition zone and its implications for global material circulation, *Earth Planet. Sci. Lett.*, *301*(3-4), 413–423, doi:10.1016/j.epsl.2010.11.038.
Karato, S., and D. Wang (2013), Electrical conductivity of minerals and rocks, in *Physics and Chemistry of the Deep Earth*, edited by S. Karato, pp. 145–236, John Wiley & Sons, Ltd., Chichester, West Sussex, U. K.
Kind, R., and X. Yuan (2010), Seismic Images of the Biggest Crash on Earth, *Science*, *329*, 1479–1480.
Kind, R., et al. (2002), Seismic images of crust and upper mantle beneath Tibet: Evidence for Eurasian plate subduction, *Science*, *298*, 1219–1221, doi:10.1126/science.1078115.
Klemperer, S. L. (2006), Crustal flow in Tibet: Geophysical evidence for the physical state of Tibetan lithosphere, and inferred patterns of active flow, *Geol. Soc. Spec. Publ.*, *268*(1), 39–70, doi:10.1144/GSL.SP.2006.268.01.03.
Kovács, I., D. H. Green, A. Rosenthal, J. Hermann, H. S. C. O'neill, W. O. Hibberson, and B. Udvardi (2012), An experimental study of water in nominally anhydrous minerals in the upper mantle near the water-saturated solidus, *J. Petrol.*, *53*(10), 2067–2093, doi:10.1093/petrology/egs044.
Kumar, P., X. Yuan, R. Kind, and J. Ni (2006), Imaging the colliding Indian and Asian lithospheric plates beneath Tibet, *J. Geophys. Res.*, *111*, B06308, doi:10.1029/2005JB003930.
Lee, C.-T. a., P. Luffi, and E. J. Chin (2011), Building and destroying continental mantle, *Annu. Rev. Earth Planet. Sci.*, *39*(1), 59–90, doi:10.1146/annurev-earth-040610-133505.
Leech, M. L. (2001), Arrested orogenic development: Eclogitization, delamination, and tectonic collapse, *Earth Planet. Sci. Lett.*, *185*(1-2), 149–159, doi:10.1016/S0012-821X(00)00374-5.
Li, C., R. D. van der Hilst, A. S. Meltzer, and E. R. Engdahl (2008a), Subduction of the Indian lithosphere beneath the Tibetan Plateau and Burma, *Earth Planet. Sci. Lett.*, *274*(1-2), 157–168, doi:10.1016/j.epsl.2008.07.016.
Li, S., M. J. Unsworth, J. R. Booker, W. Wei, H. Tan, and A. G. Jones (2003), Partial melt or aqueous fluid in the mid-crust of Southern Tibet? Constraints from INDEPTH magnetotelluric data, *Geophys. J. Int.*, *153*, 289–304.
Li, Y., Q. Wu, X. Tian, R. Zeng, R. Zhang, and H. Li (2006), Crustal structure beneath Qiangtang and Lhasa terrane from receiver function, *Acta Seismol. Sin.*, *19*(6), 633–642, doi:10.1007/s11589-006-0633-z.
Li, Z.-X. A., C.-T. a. Lee, A. H. Peslier, A. Lenardic, and S. J. Mackwell (2008b), Water contents in mantle xenoliths from the Colorado Plateau and vicinity: Implications for the mantle rheology and hydration-induced thinning of continental lithosphere, *J. Geophys. Res.*, *113*, B09210, doi:10.1029/2007JB005540.
Liang, X., E. Sandvol, Y. J. Chen, T. Hearn, J. Ni, S. L. Klemperer, Y. Shen, and F. Tilmann (2012), A complex Tibetan upper mantle: A fragmented Indian slab and no south-verging subduction of Eurasian lithosphere, *Earth Planet. Sci. Lett.*, *333–334*, 101–111, doi:10.1016/j.epsl.2012.03.036.
Liu, C.-Z., F.-Y. Wu, S.-L. Chung, and Z.-D. Zhao (2011), Fragments of hot and metasomatized mantle lithosphere in Middle Miocene ultrapotassic lavas, southern Tibet, *Geology*, *39*(10), 923–926, doi:10.1130/G32172.1.

© 2014. American Geophysical Union. All Rights Reserved.

Martí, A., P. Queralt, and J. Ledo (2009), WALDIM: A code for the dimensionality analysis of magnetotelluric data using the rotational invariants of the magnetotelluric tensor, *Comput. Geosci.*, *35*(12), 2295–2303, doi:10.1016/j.cageo.2009.03.004.
McDonough, W. F., and S.-S. Sun (1995), The composition of the Earth, *Chem. Geol.*, *120*, 223–253.
McKenzie, D., and K. Priestley (2008), The influence of lithospheric thickness variations on continental evolution, *Lithos*, *102*, 1–11, doi:10.1016/j.lithos.2007.05.005.
McKenzie, D., J. Jackson, and K. Priestley (2005), Thermal structure of oceanic and continental lithosphere, *Earth Planet. Sci. Lett.*, *233*(3-4), 337–349, doi:10.1016/j.epsl.2005.02.005.
McNamara, D. E., T. J. Owens, and R. Walter, William (1995), Observations of regional phase propagation across the Tibetan Plateau, *J. Geophys. Res.*, *100*(B11), 22,215–22,229.
McNeice, G. W., and A. G. Jones (2001), Multisite, multifrequency tensor decomposition of magnetotelluric data, *Geophysics*, *66*(1), 158–173.
Mechie, J., S. V. Sobolev, L. Ratschbacher, A. Y. U. Babeyko, G. Bock, A. G. Jones, K. D. Nelson, K. D. Solon, L. D. Brown, and W. Zhao (2004), Precise temperature estimation in the Tibetan crust from seismic detection of the α-β quartz transition, *Geology*, *32*(7), 601, doi:10.1130/G20367.1.
Minster, J. B., and D. L. Anderson (1981), A model of dislocation controlled rheology for the mantle, *Philos. Trans. R. Soc. London A*, *299*, 319–356, doi:10.1098/rsta.1981.0025.
Molnar, P., and P. Tapponnier (1977), Relation of the tectonics of eastern China to the India-Eurasia collision: Application of slip-line field theory to large-scale continental tectonics, *Geology*, *5*, 212–216.
Molnar, P., P. C. England, and J. Martinod (1993), Mantle dynamics, uplift of the Tibetan Plateau, and the Indian monsoon, *Rev. Geophys.*, *31*(4), 357–396.
Monsalve, G., a. Sheehan, V. Schulte-Pelkum, S. Rajaure, M. R. Pandey, and F. Wu (2006), Seismicity and one-dimensional velocity structure of the Himalayan collision zone: Earthquakes in the crust and upper mantle, *J. Geophys. Res.*, *111*, B10301, doi:10.1029/2005JB004062.
Nábělek, J. L., G. Hetényi, J. Vergne, S. Sapkota, B. Kafle, J. Mei, H. Su, J. Y. Chen, B.-S. Huang, and H.-C. Team (2009), Underplating in the Himalaya-Tibet collision zone revealed by the Hi-CLIMB experiment, *Science*, *325*, 1371–1374, doi:10.1126/science.1167719.
Nelson, K. D., et al. (1996), Partially molten middle crust beneath southern Tibet: Synthesis of project INDEPTH results, *Science*, *274*, 1684–1688.
Ni, J., and M. Barazangi (1984), Seismotectonics of the Himalayan collision zone: Geometry of the underthrusting Indian plate beneath the Himalaya, *J. Geophys. Res.*, *89*(3), 1147–1163.
Nunn, C., S. W. Roecker, F. Tilmann, K. Priestley, R. Heyburn, E. Sandvol, J. Ni, Y. J. Chen, W. Zhao, and the I. I. Team (2013), Imaging the lithosphere beneath NE Tibet: Tteleseismic P and S body wave tomography incorporating surface wave starting models, *Geophys. J. Int.*, *196*(3), 1724–1741, doi:10.1093/gji/ggt476.
Owens, T. J., and G. Zandt (1997), Implications of crustal property variations for models of Tibetan plateau evolution, *Nature*, *387*, 37–43.
Owens, T. J., G. E. Randall, F. T. Wu, and R. Zeng (1993), PASSCAL instrument performance during the Tibetan Plateau passive seismic experiment, *Bull. Seismol. Soc. Am.*, *83*(6), 1959–1970.
Le Pape, F., A. G. Jones, J. Vozar, and W. Wenbo (2012), Penetration of crustal melt beyond the Kunlun Fault into northern Tibet, *Nat. Geosci.*, *5*(5), 1–6, doi:10.1038/ngeo1449.
Parker, R. L., and J. R. Booker (1996), Optimal one-dimensional inversion and bounding of magnetotelluric apparent resistivity and phase measurements, *Phys. Earth Planet. Inter.*, *98*(3-4), 269–282, doi:10.1016/S0031-9201(96)03191-3.
Partzsch, G. M., and F. R. Schilling (2000), The influence of partial melting on the electrical behavior of crustal rocks: Laboratory examinations, model calculations and geological interpretations, *Tectonophysics*, *317*(3-4), 189–203, doi:10.1016/S0040-1951(99)00320-0.
Peslier, A. H. (2010), A review of water contents of nominally anhydrous natural minerals in the mantles of Earth, Mars and the Moon, *J. Volcanol. Geotherm. Res.*, *197*(1-4), 239–258, doi:10.1016/j.jvolgeores.2009.10.006.
Peslier, A. H., A. B. Woodland, D. R. Bell, and M. Lazarov (2010), Olivine water contents in the continental lithosphere and the longevity of cratons., *Nature*, *467*(7311), 78–81, doi:10.1038/nature09317.
Pham, V. N., D. Boyer, P. Therme, X. Yuan, and L. Li (1986), Partial melting zones in the crust in southern Tibet from magnetotelluric results, *Nature*, *319*, 310–314.
Platt, J. P., and P. C. England (1994), Convective removal of lithosphere beneath mountain belts: Thermal and mechanical consequences, *Am. J. Sci.*, *294*, 307–336.
Poe, B. T., C. Romano, F. Nestola, and J. R. Smyth (2010), Electrical conductivity anisotropy of dry and hydrous olivine at 8GPa, *Phys. Earth Planet. Inter.*, *181*(3-4), 103–111, doi:10.1016/j.pepi.2010.05.003.
Pollack, H. N., S. J. Hurter, and J. R. Johnson (1993), Heat flow from the Earth's interior: Analysis of the global data set, *Rev. Geophys.*, *31*(3), 267–280.
Pommier, a., and E. Le-Trong (2011), "SIGMELTS": A web portal for electrical conductivity calculations in geosciences, *Comput. Geosci.*, *1–10*, doi:10.1016/j.cageo.2011.01.002.
Priestley, K., J. James, and D. McKenzie (2008), Lithospheric structure and deep earthquakes beneath India, the Himalaya and southern Tibet, *Geophys. J. Int.*, *172*(1), 345–362.
Rapine, R. (2003), Crustal structure of northern and southern Tibet from surface wave dispersion analysis, *J. Geophys. Res.*, *108*(B2), 2120, doi:10.1029/2001JB000445.
Rippe, D., and M. J. Unsworth (2010), Quantifying crustal flow in Tibet with magnetotelluric data, *Phys. Earth Planet. Inter.*, *179*(3-4), 107–121, doi:10.1016/j.pepi.2010.01.009.
Ross, A. R., L. D. Brown, P. Pananont, K. D. Nelson, S. L. Klemperer, S. Haines, Z. Wenjin, and G. Jingru (2004), Deep reflection surveying in central Tibet: Lower-crustal layering and crustal flow, *Geophys. J. Int.*, *156*(1), 115–128, doi:10.1111/j.1365-246X.2004.02119.x.
Royden, L. H., B. C. Burchfiel, R. W. King, E. Wang, Z. Chen, F. Shen, and Y. Liu (1997), Surface Deformation and Lower Crustal Flow in Eastern Tibet, *Science*, *276*(5313), 788–90.
Royden, L. H., B. C. Burchfiel, and R. D. van der Hilst (2008), The geological evolution of the Tibetan Plateau., *Science*, *321*(5892), 1054–8, doi:10.1126/science.1155371.
Sandvol, E., J. Chen, J. Ni, S. Zhou, Y. Ma, X. Zhang, H. Yue, S. Ceylan, X. C. Bao, and T. Hearn (2008), Lithospheric Seismic Velocity Structure of the Northern Tibetan Plateau: The ASCENT Seismic Experiment, *Eos Trans. AGU*, *89*(53), Fall Meet. Suppl., Abstract S14A–01.
Searle, M. P., J. Elliott, R. Phillips, and S.-L. Chung (2011), Crustal-lithospheric structure and continental extrusion of Tibet, *J. Geol. Soc.*, *168*(3), 633, doi:10.1144/0016-76492010-139.Crustal.
Shen, F., L. H. Royden, and B. C. Burchfiel (2001), Large-scale crustal deformation of the Tibetan Plateau, *J. Geophys. Res.*, *106*, 6793–6816.
Schaeffer, A. J., and S. Lebedev (2013), Global shear speed structure of the upper mantle and transition zone, *Geophys. J. Int.*, *194*(1), 417–449, doi:10.1093/gji/ggt095.

© 2014. American Geophysical Union. All Rights Reserved.

Simpson, F., and K. Bahr (2005), *Practical Magnetotellurics*, Cambridge Univ. Press, Cambridge, U. K.
Sol, S., et al. (2007), Geodynamics of the southeastern Tibetan Plateau from seismic anisotropy and geodesy, *Geology*, *35*(6), 563–566, doi:10.1130/G23408A.1.
Solon, K. D., A. G. Jones, D. Nelson, M. J. Unsworth, W. S. F. Kidd, and W. Wei (2005), Structure of the crust in the vicinity of the Banggong-Nujiang suture in central Tibet from INDEPTH magnetotelluric data, *J. Geophys. Res.*, *110*, B10102, doi:10.1029/2003JB002405.
Spratt, J. E., A. G. Jones, D. Nelson, M. J. Unsworth, and the I. M. Team (2005), Crustal structure of the India-Asia collision zone, southern Tibet, from INDEPTH MT investigations, *Phys. Earth Planet. Inter.*, *150*(1-3), 227–237, doi:10.1016/j.pepi.2004.08.035.
Tao, W., and Z. Shen (2008), Heat flow distribution in Chinese continent and its adjacent areas, *Prog. Nat. Sci.*, *18*(7), 843–849, doi:10.1016/j.pnsc.2008.01.018.
Tapponnier, P., X. Zhiqin, F. Roger, B. Meyer, N. Arnaud, G. Wittlinger, and Y. Jingsui (2001), Oblique stepwise rise and growth of the Tibet plateau., *Science*, *294*(5547), 1671–7, doi:10.1126/science.105978.
Taylor, M. (2003), Conjugate strike-slip faulting along the Bangong-Nujiang suture zone accommodates coeval east-west extension and north-south shortening in the interior of the Tibetan Plateau, *Tectonics*, *22*(4), 1044, doi:10.1029/2002TC001361.
Tenner, T. J., M. M. Hirschmann, A. C. Withers, and R. L. Hervig (2009), Hydrogen partitioning between nominally anhydrous upper mantle minerals and melt between 3 and 5 GPa and applications to hydrous peridotite partial melting, *Chem. Geol.*, *262*(1-2), 42–56, doi:10.1016/j.chemgeo.2008.12.006.
Tilmann, F., J. Ni, and I. I. S. Team (2003), Seismic imaging of the downwelling Indian lithosphere beneath central Tibet, *Science*, *300*, 1424–1427.
Unsworth, M. J., et al. (2005), Crustal rheology of the Himalaya and Southern Tibet inferred from magnetotelluric data., *Nature*, *438*(7064), 78–81, doi:10.1038/nature04154.
Wang, D., M. Mookherjee, Y. Xu, and S. Karato (2006), The effect of water on the electrical conductivity of olivine., *Nature*, *443*(7114), 977–80, doi:10.1038/nature05256.
Wang, Q., et al. (2001), Present-day crustal deformation in China constrained by global positioning system measurements., *Science*, *294*(5542), 574–7, doi:10.1126/science.1063647.
Wang, Y. (2001), Heat flow pattern and lateral variations of lithosphere strength in China mainland: Constraints on active deformation, *Phys. Earth Planet. Inter.*, *126*(3-4), 121–146, doi:10.1016/S0031-9201(01)00251-5.
Wei, W., et al. (2001), Detection of widespread fluids in the Tibetan crust by magnetotelluric studies., *Science*, *292*(5517), 716–9, doi:10.1126/science.1010580.
Wei, W., et al. (2014), Northward Channel flow in Northern Tibet revealed from 3D magnetotelluric modelling, *Phys. Earth Planet. Inter.*, *235*, 13–24, doi:10.1016/j.pepi.2014.07.004.
Willett, S. D., and C. Beaumont (1994), Subduction of Asian lithospheric mantle beneath Tibet inferred from models of continental collision, *Nature*, *369*, 642–645.
Williams, H. M., S. Turner, J. A. Pearce, S. Kelley, and N. B. Harris (2004), Nature of the Source Regions for Post-collisional, Potassic Magmatism in Southern and Northern Tibet from Geochemical Variations and Inverse Trace Element Modelling, *J. Petrol.*, *45*(3), 555–607, doi:10.1093/petrology/egg094.
Wittlinger, G., V. Farra, and J. Vergne (2004), Lithospheric and upper mantle stratifications beneath Tibet: New insights from Sp conversions, *Geophys. Res. Lett.*, *31*, L19615, doi:10.1029/2004GL020955.
Xia, Q.-K., Y. Hao, P. Li, E. Deloule, M. Coltorti, L. Dallai, X. Yang, and M. Feng (2010), Low water content of the Cenozoic lithospheric mantle beneath the eastern part of the North China Craton, *J. Geophys. Res.*, *115*, B07207, doi:10.1029/2009JB006694.
Xiong, X., R. Gao, Q. Li, Z. Lu, X. Xiaosong, G. Rui, L. Qiusheng, and L. Zhanwu (2009), Moho depth of Qinghai-Tibet plateau revealed by seismic probing, *J. Earth Sci.*, *20*(2), 448–463, doi:10.1007/s12583-009-0037-9.
Xu, L., S. Rondenay, and R. D. van der Hilst (2007), Structure of the crust beneath the southeastern Tibetan Plateau from teleseismic receiver functions, *Phys. Earth Planet. Inter.*, *165*(3-4), 176–193, doi:10.1016/j.pepi.2007.09.002.
Yang, Y., M. H. Ritzwoller, Y. Zheng, W. Shen, A. L. Levshin, and Z. Xie (2012), A synoptic view of the distribution and connectivity of the mid-crustal low velocity zone beneath Tibet, *J. Geophys. Res.*, *117*, B04303, doi:10.1029/2011JB008810.
Yin, A., and T. M. Harrison (2000), Geologic Evolution of the Himalayan-Tibetan Orogen, *Annu. Rev. Earth Planet. Sci.*, *28*(1), 211–280, doi:10.1146/annurev.earth.28.1.211.
Yoshino, T. (2010), Laboratory electrical conductivity measurement of mantle minerals, *Surv. Geophys.*, *31*(2), 163–206, doi:10.1007/s10712-009-9084-0.
Yoshino, T., T. Matsuzaki, A. Shatskiy, and T. Katsura (2009), The effect of water on the electrical conductivity of olivine aggregates and its implications for the electrical structure of the upper mantle, *Earth Planet. Sci. Lett.*, *288*(1-2), 291–300, doi:10.1016/j.epsl.2009.09.032.
Yue, H., et al. (2012), Lithospheric and upper mantle structure of the northeastern Tibetan Plateau, *J. Geophys. Res.*, *117*, B05307, doi:10.1029/2011JB008545.
Yuen, D. A., S. Maruyama, S.-I. Karato, and B. F. Windley (Eds.) (2007), *Superplumes: Beyond Plate Tectonics*, Springer, Dordrecht, Netherlands.
Zhang, Z., and S. L. Klemperer (2010), Crustal structure of the Tethyan Himalaya, southern Tibet: New constraints from old wide-angle seismic data, *Geophys. J. Int.*, 1247–1260, doi:10.1111/j.1365-246X.2010.04578.x.
Zhao, J., et al. (2010), The boundary between the Indian and Asian tectonic plates below Tibet., *Proc. Natl. Acad. Sci. U. S. A.*, *107*(25), 11229–33, doi:10.1073/pnas.1001921107.
Zhao, W., et al. (2001), Crustal structure of central Tibet as derived from project INDEPTH wide-angle seismic data, *Geophys. J. Int.*, *145*, 486–498.
Zhao, W., L. D. Brown, Z. Wu, S. L. Klemperer, D. Shi, J. Mechie, H. Su, F. Tilmann, M. S. Karplus, and Y. Makovsky (2008), Seismology across the northeastern edge of the Tibetan Plateau, *Eos Trans. AGU*, *89*(48), 487–488.
Zhao, W., et al. (2011), Tibetan plate overriding the Asian plate in central and northern Tibet, *Nat. Geosci.*, *4*(12), 870–873, doi:10.1038/ngeo1309.
Zheng, Y.-F., Q.-X. Xia, R.-X. Chen, and X.-Y. Gao (2011), Partial melting, fluid supercriticality and element mobility in ultrahigh-pressure metamorphic rocks during continental collision, *Earth Sci. Rev.*, *107*(3-4), 342–374, doi:10.1016/j.earscirev.2011.04.004.
Zhu, D.-C., X.-X. Mo, Y. Niu, Z.-D. Zhao, L.-Q. Wang, G.-T. Pan, and F.-Y. Wu (2009), Zircon U–Pb dating and in-situ Hf isotopic analysis of Permian peraluminous granite in the Lhasa terrane, southern Tibet: Implications for Permian collisional orogeny and paleogeography, *Tectonophysics*, *469*(1-4), 48–60, doi:10.1016/j.tecto.2009.01.017.

© 2014. American Geophysical Union. All Rights Reserved.